1. KONFERENCIA ZDRAVOTNÝ KOMPAS

1. Konferencia Zdravotného Kompasu

s hlavnou témou

Využitie dátovej analytiky v biomedicínskom výskume

ZBORNÍK ROZŠÍRENÝCH ABSTRAKTOV

Miesto konania konferencie: Centrum experimentálnej medicíny SAV, Bratislava
Dúbravská cesta 9, 841 04 Bratislava, Slovensko
Dátum konania konferencie: 28. júl 2025

Organizátor:
Heger s.r.o.

Partneri:
Centrum experimentálnej medicíny Slovenskej akadémie vied
Prírodovedecká fakulta Univerzity Komenského v Bratislave

CENTRUM EXPERIMENTÁLNEJ MEDICÍNY SLOVENSKEJ AKADÉMIE VIED

PRÍRODOVEDECKÁ FAKULTA
Univerzita Komenského
v Bratislave

Úvodné slovo

Vážené čitateľky, vážení čitatelia,
s hrdosťou a veľkým očakávaním Vám predkladáme tento Zborník rozšírených abstraktov, ktorý vzišiel z **historicky prvého ročníka Konferencie Zdravotného Kompasu**. Stojíme na začiatku niečoho nového a naším úprimným želaním je, aby sa toto podujatie stalo pevnou tradíciou – miestom pravidelného stretávania sa vedeckej komunity, výmeny poznatkov a inšpirácie.
Téma „Využitie dátovej analytiky v biomedicínskom výskume“ nebola zvolená náhodne. Žijeme v dobe, kedy sa dáta stávajú novým mikroskopom, ktorý nám umožňuje nahliadnuť do zložitých biologických procesov s nevídanou presnosťou. Správna interpretácia obrovského množstva dát generovaných v medicíne a biológii otvára dvere k personalizovanej liečbe, prediktívnej diagnostike a efektívnejšiemu vývoju liečiv.
Uskutočnenie tejto konferencie a vydanie tohto zborníka by nebolo možné bez významnej podpory našich partnerov – **Centra experimentálnej medicíny Slovenskej akadémie vied** a **Prírodovedeckej fakulty Univerzity Komenského v Bratislave**. Patrí im naša úprimná vďaka. Rovnako ďakujeme všetkým autorom, ktorých príspevky tvoria jadro tohto zborníka, ako aj recenzentom za ich odborný dohľad.
Pevne veríme, že sa nám podarilo založiť tradíciu, ktorá bude z roka na rok silnieť a ktorá bude do budúcna priťahovať **stále viac prác na čoraz vyššej odbornej úrovni**. Veríme, že aj vy, čitatelia, nájdete v predložených abstraktoch cenné podnety pre svoju vlastnú prácu.
Želáme vám podnetné a obohacujúce čítanie.
S úctou,

Mgr. Vladimír Heger, PhD.
za organizačný výbor (Heger s.r.o.)

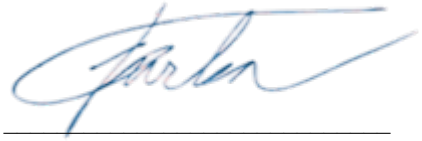

Mgr. Samuel Furka, PhD., MLJ.
Spoluorganizátor a recenzent
(Prírodovedecká fakulta univerzity Komenského v Bratislave)

Mgr. Daniel Furka, PhD., MLJ.
Spoluorganizátor a recenzent
(Prírodovedecká fakulta univerzity Komenského v Bratislave)

Program Konferencie

9:30 – 9:50 Registrácia a príchod účastníkov

9:50 – 10:00 Otvorenie konferencie a úvodné slovo organizátorov

BLOK I: Materiálové inovácie a dátová analýza v biomedicíne: od nanoštruktúr po klinické aplikácie

10:00 – 11:00 Prednášky:

1. Clinical 3D printing in medicine - overview and trends
2. Kinetics of photocatalysis of metal oxide-based nanomaterials
3. Surface-Modified Polymer Optical Fibres with Anisotropic Properties for Real-Time Biomechanical Sensing
4. Innovative composite materials with surface modification, optimized microtopography, thermal conductivity and mechanical properties for the design of artificial tissues and their interfaces
5. Study of Composite Conductive Layers Based on Graphite and Doped ZnO Nanoparticles For Sensor Integration into 3D-Printed Cardiac Valves and Vascular Structures
6. Biochemical Diagnosis of Congenital Adrenal Hyperplasia Using Mass Spectrometry-Based Methods

10:50 – 11:00 Diskusia k Bloku I

BLOK II: Dáta, algoritmy, rozhodnutia: AI a analytika v službách biomedicíny

11:00 – 11:50 Prednášky:

1. AI-Assisted Profiling of multidimensional data for Gut Phenotype Classification: Development and Validation of the QUANTUM Diagnostic Platform.
2. Comparative Analysis of Artificial Intelligence Model Architectures: Strengths, Limitations, and Application Domains.
3. Integrácia prediktívnych nástrojov do manažmentu antibiotickej liečby (AMS)
4. Dátové inžinierstvo v biomedicíne pomocou KNIME: Skúsenosti zo Zdravotného Kompasu
5. Zdravotný Kompas a Vedecký Radar: Informačná inteligencia pre biomedicínsky výskum

11:50 – 12:00 Diskusia k Bloku II

12:00 Záverečné slovo a ukončenie konferencie

Nasleduje Občerstvenie, voľná diskusia a networking


BLOK I
Materiálové inovácie
a dátová analýza
v biomedicíne:
od nanoštruktúr
po klinické aplikácie

Clinical 3D printing in medicine - overview and trends

Samuel Furka [1] , Daniel Furka [1],

[1] *Comenius University, Faculty of Natural Sciences, Department of Physical and Theoretical Chemistry, Ilkovičova 3220/6, 84215 Bratislava, Slovakia*

Clinical 3D printing has emerged as a revolutionary technology in modern medicine, offering transformative applications across various healthcare domains. By leveraging advanced additive manufacturing techniques, 3D printing enables the creation of highly accurate, patient-specific anatomical models, surgical tools, and implants, leading to enhanced precision in diagnosis, treatment planning, and surgical procedures. The ability to produce customized prosthetics and implants tailored to individual patients has significantly improved outcomes, particularly in orthopedics, maxillofacial surgery, and reconstructive procedures.

In surgical planning, 3D-printed models derived from medical imaging data (such as CT or MRI scans) provide surgeons with a tangible, three-dimensional representation of a patient's anatomy, facilitating better preoperative preparation, reducing operative time, and minimizing complications. The advent of bioprinting an extension of 3D printing has further opened new frontiers in regenerative medicine, including the development of bio-printed tissues and organs, offering potential solutions to organ shortages.

Additionally, the integration of 3D printing into medical education and training has allowed for more realistic simulation of complex surgical procedures, enhancing learning and proficiency. The growing availability of affordable 3D printers and advances in materials science are further driving the adoption of this technology, making it increasingly accessible to healthcare facilities worldwide.

Despite its potential, challenges remain, such as regulatory hurdles, standardization of materials, and the need for long-term clinical validation. Nevertheless, the future of clinical 3D printing in medicine holds immense promise, with its capacity to personalize healthcare, improve patient outcomes, and transform the way medical procedures are performed.

Acknowledgement: The authors gratefully acknowledge the financial and institutional support provided by the Slovak Agency for International Development Cooperation (SAMRS) and the Ministry of Foreign and European Affairs of the Slovak Republic. We also extend our sincere thanks to PerBiotiX s.r.o. for providing anonymised stool samples and for their collaboration in sample collection and preparation. This project "Improving public health by sending doctors, community education, providing internships and deploying an AI disease analyser and water purification equipment (SAMRS/2024/KE/1/2)" lasting from 12.2024 to 04.2026 is implemented with funds from the official development assistance of the Slovak Republic.

Kinetics of photocatalysis of metal oxide-based nanomaterials

Mária Martinická[1], Viktória Pohorelská[1] , Daniel Furka[1]

[1] *Department of Physical and Theoretical Chemistry, Faculty of Natural Sciences, Comenius University in Bratislava, Mlynska dolina, Ilkovicova 6, 842 15 Bratislava 4, Slovakia*

Photocatalysis, a light-driven process leveraging semiconductor nanomaterials, has emerged not only as a method for environmental detoxification but also as a platform for biomedical applications including antimicrobial treatment and photodynamic therapy. Central to these technologies is the ability of metal oxide nanoparticles to generate reactive oxygen species (ROS) under light irradiation, triggering oxidative degradation of organic structures. In this context, understanding how material properties influence ROS-mediated reactions is essential. This study investigates four common metal oxide photocatalysts—ZnO, TiO_2, V_2O_5, and Fe_2O_3—under standardized UV-LED exposure, using phloxine B as a model compound. By exploring their structural, optical, and kinetic characteristics, the work contributes insights relevant to both environmental engineering and nanomedicine.

1. Introduction

Synthetic dyes are frequently discharged into aquatic ecosystems through industrial effluents, where they resist biodegradation and accumulate due to their stable molecular structures. These pollutants can disrupt aquatic life and pose potential health risks if they enter drinking water sources. Conventional treatment methods often fail to eliminate such persistent organic compounds. Photocatalytic degradation, which utilizes semiconductor metal oxide nanoparticles to harness light energy and generate ROS, offers an effective strategy for dye mineralization. In this study, zinc oxide (ZnO), titanium dioxide (TiO_2), vanadium pentoxide (V_2O_5), and iron(III) oxide (Fe_2O_3) nanoparticles were selected for comparative evaluation. Their photocatalytic activity was assessed through the degradation of phloxine B, a representative xanthene dye, under UV-LED irradiation. The aim was to determine how differences in crystal structure, bandgap energy, and surface characteristics affect degradation efficiency and kinetic behavior.

2. Materials and Methods

X-ray powder diffraction (PXRD) was performed using a URD 6 diffractometer (Seifert FPM GmbH, Germany) equipped with a copper Kα radiation source (λ = 0.154187 nm). The diffraction data were collected in the 2θ range of 25° to 80°, with an exposure time of 1 second per step. The crystalline structure of the nanoparticles was analyzed using MATCH!© software (Crystal Impact GbR, Germany). Infrared absorption spectra were obtained using a Nicolet 6700 FTIR spectrometer in ATR mode (Thermo Electron Corp., USA). UV-Vis absorption spectra were recorded using a FURKALAB FL80P spectrophotometer at 30-minute intervals over a 24-hour period. Measurements were conducted at a constant temperature of 26 °C in standard quartz cuvettes. Phloxine B solutions were prepared by dissolving 20.71 mg of the sodium salt of phloxine B (Mw = 829.63 g/mol) in distilled, deionized water to make a 0.1

mmol·dm^{-3} stock solution in a 250 mL volumetric flask. Calibration solutions for photolysis evaluation were prepared in concentrations ranging from 1×10^{-6} to 1×10^{-4} mol·dm^{-3}. Commercially available, high-purity metal oxide nanoparticles were used in the experiments. ZnO, TiO_2, and Fe_2O_3 nanoparticles were purchased from Nanografi (Turkey), while V_2O_5 nanoparticles were obtained from INSCX (Ireland). The ZnO nanoparticles (NG10DNPW0992) had a size of 20–30 nm and hexagonal morphology. TiO_2 nanoparticles (NG10NPW0931) were P25 type and 20 nm in size. Fe_2O_3 nanoparticles (NG04SO1404) ranged from 18 to 38 nm in size with spherical morphology. V_2O_5 nanoparticles (NS6130-03-399) measured 80 nm and had an orthorhombic crystal structure. All solutions and dispersions were prepared using distilled, deionized water obtained by reverse osmosis with a resistivity of 18.1 MΩ. The photocatalytic degradation of phloxine B was studied by preparing dispersions of 250 mg of each photocatalyst in an aqueous solution of phloxine B at a concentration of 1×10^{-4} mol·dm^{-3}. These dispersions were placed in quartz cuvettes, where the nanoparticles were allowed to settle, and the samples were irradiated from below using a UV-LED source (365 nm, 10 mW) for 24 hours. Control experiments showed that direct photolysis of phloxine B under UV light without catalyst was negligible (0.05% over 24 hours), and that adsorption of dye onto the nanoparticles in the absence of light was not statistically significant. The absorbance of the dye solution was measured spectrophotometrically at hourly intervals throughout the irradiation period. This allowed for monitoring the time-dependent degradation of phloxine B and for evaluating the photocatalytic activity of each nanoparticle type by quantifying the decrease in absorbance at the dye's characteristic maximum.

3. Results

X-ray diffraction analysis confirmed that each photocatalyst possessed the expected crystalline phase, supporting their structural integrity for photocatalytic applications. ATR-FTIR spectroscopy further validated the material identities by displaying the characteristic vibrational modes of metal–oxygen bonds. Optical bandgap characterization revealed notable differences among the photocatalysts. ZnO and TiO_2 exhibited wide bandgaps of 3.14 eV and 3.25 eV, respectively, while V_2O_5 showed a narrower bandgap of 2.41 eV. The optical bandgap of Fe_2O_3 could not be reliably determined due to the lack of a clearly defined absorption edge, likely stemming from complex electronic transitions. These variations in bandgap correlate with differences in light absorption and electron–hole generation efficiencies. Photocatalytic performance varied significantly across the materials. ZnO achieved the most effective degradation of phloxine B, removing 75.5% of the dye, followed by TiO_2 at 66.6%, V_2O_5 at 47.3%, and Fe_2O_3 at 20.5%. Kinetic analysis indicated that degradation in the ZnO and TiO_2 systems followed first-order reaction behavior, suggesting a direct proportionality between dye concentration and reaction rate. In contrast, second-order kinetics best described the behavior of V_2O_5 and Fe_2O_3, implying more complex reaction dynamics possibly involving surface interactions or adsorption processes. Deviations from ideal kinetic models became evident at later reaction stages, characterized by reduced degradation rates. These were likely caused by diminished dye concentration, accumulation of degradation intermediates on catalyst surfaces, reduced light penetration, and inhibitory effects from by-products.

4. Discussion

The differences in photocatalytic activity are primarily attributed to variations in bandgap energy and the efficiency of charge carrier generation and separation. ZnO and TiO_2 exhibited superior performance due to more efficient generation and transfer of electron–hole pairs, enhancing ROS production that drives oxidative dye degradation. The underlying mechanism

involves absorption of photons with energy equal to or greater than the bandgap, creating electron-hole pairs. The holes oxidize water or hydroxide ions to produce hydroxyl radicals, while electrons reduce oxygen molecules to superoxide radicals. The synergistic action of these reactive species results in the mineralization of the dye. The molecular breakdown of phloxine B involves cleavage of phenolate groups and halogen substituents, as reported in prior studies [1]. These structural moieties are susceptible to attack by reactive radicals generated during photocatalysis, leading to stepwise degradation into smaller, less toxic fragments. Photocatalytic degradation disrupts the π-conjugated system of the dye molecule, thereby eliminating its ability to absorb light in the visible region, which is observed as the loss of color.

5. Conclusions

This study demonstrates that the photocatalytic degradation efficiency of metal oxide nanoparticles is strongly influenced by their bandgap energy and associated charge carrier dynamics. ZnO and TiO_2 outperformed V_2O_5 and Fe_2O_3 in both degradation rates and overall dye removal efficiency, correlating with more favorable electronic properties for ROS generation. The kinetic profiles further revealed differences in reaction mechanisms, underscoring the need for catalyst-specific modeling approaches. These findings emphasize the importance of material selection and optical tuning in designing photocatalysts for environmental remediation. Beyond wastewater treatment, the observed principles may inform the development of ROS-based biomedical technologies, such as photodynamic therapy or antimicrobial surfaces. Future work should focus on improving photocatalyst performance under visible light and elucidating degradation pathways through advanced analytical techniques.

References

1. L. Wang, W. F. Cai, and Q. X. Li, “Photolysis of phloxine B in water and aqueous solutions,” *Arch Environ Contam Toxicol*, vol. 35, no. 3, 1998, doi: 10.1007/s002449900394.

Surface-Modified Polymer Optical Fibres with Anisotropic Properties for Real-Time Biomechanical Sensing

Jerguš Vengríni[1*], Saul Dueñas Casas[1], Andrej Tóth[1]

[1]Comenius University, Faculty of Natural Sciences, Department of Physical and Theoretical Chemistry, Mlynská dolina, Ilkovičova 6, 84104-Bratislava, Slovakia

Surface-modified polymer optical fibres (POFs) represent a promising platform for real-time biomechanical monitoring due to their light weight, flexibility and immunity to electromagnetic interference. In this study, an anisotropic tri-point POF sensor with surface-functionalised segments was developed to detect muscle-like deformation patterns under dynamic conditions. Semi-circular notches were inscribed into a polymethyl methacrylate (PMMA) fibre using a heated 3D printing nozzle and coated with spectrally distinct dye-doped elastomeric photopolymers. Finite element method (FEM) simulations optimised the notch geometry for maximal evanescent field (EF) enhancement and mechanical resilience. Spectral responses during cyclic loading were analysed using two-dimensional correlation spectroscopy (2D COS), allowing robust identification of activated sensor sites even under complex, overlapping strain fields. The sensor was integrated into a system that simulated peristaltic muscle motion using sequential pressure pulses. The approach enabled multimodal detection of strain magnitude, direction and propagation dynamics, outperforming conventional surface EMG in terms of spatial resolution and resistance to artefacts. This work demonstrates the synergistic benefits of FEM and 2D COS in accelerating the development of multipoint optical sensors for next-generation wearable applications.

1. Introduction

Polymer optical fibres have recently emerged as a versatile alternative to traditional electronic-based or silica-based strain sensors, particularly in biomedical and soft-robotic systems. [1] Their intrinsic flexibility, biocompatibility, and resistance to electromagnetic interference make them suitable for applications involving dynamic deformation in close proximity to biological tissue. However, the sensing potential of POFs remains limited unless their surface is functionally modified to allow external stimuli to influence the guided light. One effective strategy is to exploit the evanescent field (EF) at the core–cladding interface by introducing controlled surface modifications. In this context, the combination of structural design and material engineering becomes essential. Previous work has shown that introducing periodic surface notches can enhance EF leakage, thereby enabling interaction with surrounding media or coatings. [2] In parallel, functionalisation with optical dyes offers spectral encoding capabilities, paving the way for multiplexed sensing. However, the integration of these elements must consider not only the optical sensitivity but also the mechanical durability and spatial

selectivity of the fibre. This work presents a surface-modified, anisotropic POF sensor with three sensing zones, each coated with a distinct dye-doped elastomer. A comprehensive evaluation strategy based on FEM modelling and 2D correlation spectroscopy (2D COS) was employed to optimise sensor performance under conditions simulating peristaltic muscle motion. The aim was to develop a compact, multipoint sensing system capable of detecting and interpreting complex deformation dynamics in real time.

2. Materials and Methods

Commercial PMMA fibres (1 mm diameter, NA = 0.5) were modified using a custom heated 3D printing nozzle to introduce ten regularly spaced notches. Among the tested geometries, semi-circular notches offered the best balance between EF enhancement and mechanical robustness. Each notch was coated with an elastomeric photopolymer matrix incorporating one of three dyes, Phloxine B, Curcumin, or Methylene Blue, chosen for their spectrally distinct absorption and fluorescence characteristics. Coating not only introduced spectral selectivity but also improved the mechanical strength of the fibre from approximately 95 MPa to 115 MPa. FEM simulations of the LP_{01} mode on a 400 × 400 mesh revealed that semi-circular notches enhanced the EF intensity by a factor of 1.5 while maintaining mode integrity. Triangular and rectangular notches, though capable of local EF amplification, produced undesirable stress concentrations and modal distortions (Fig.1). Simulated stress maps guided the optimal orientation of the sensor such that notches faced the tensile side of the fibre during bending.

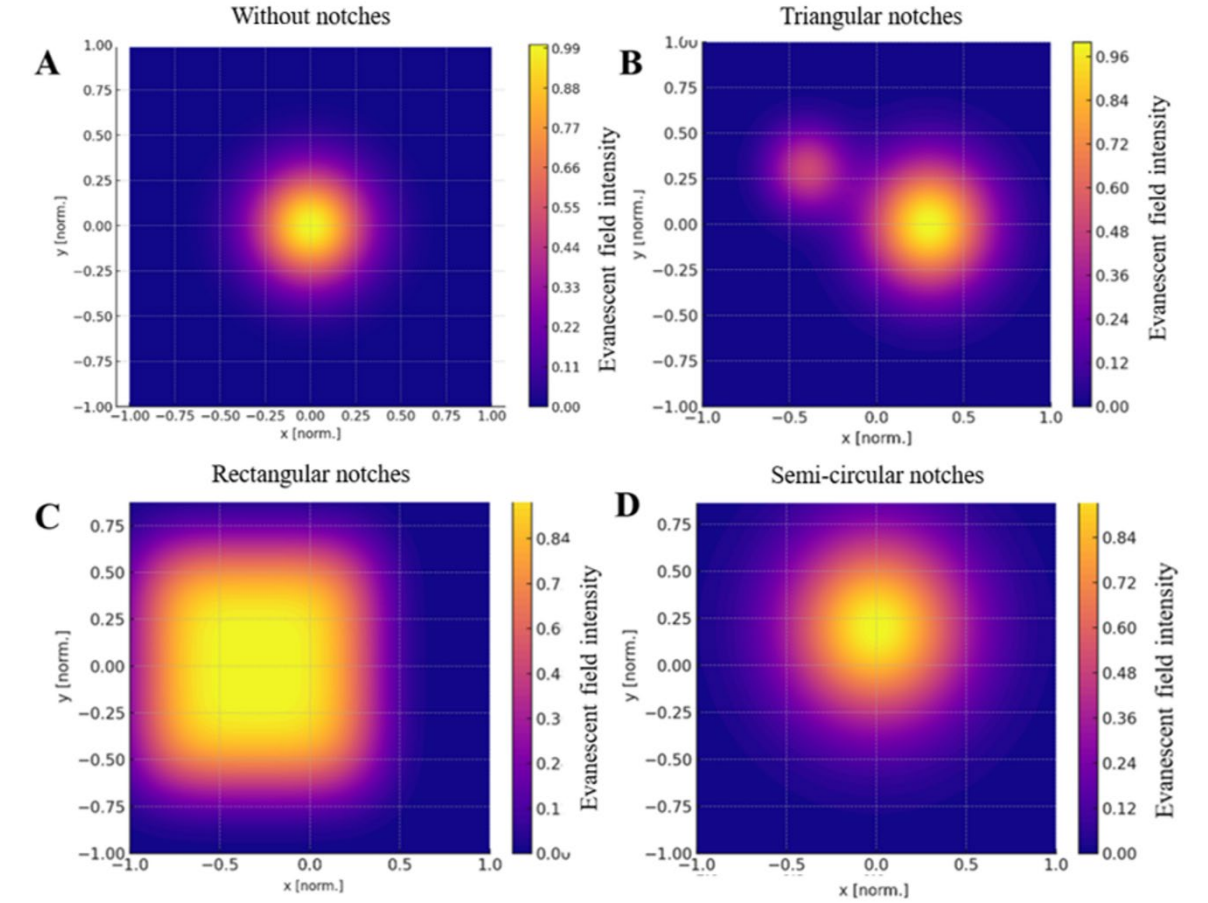

Fig.1 - FEM simulation of the evanescent field around an optical-fibre cross-section on a 400 × 400-point grid for notches of specific geometries. (A) Optical fibre without notches, (B) triangular notch geometry, (C) rectangular notch geometry, (D) semi-circular notch geometry.

Transmission spectra in the 400 nm – 700 nm range were collected under cyclic loading. The optical response of each segment included both dye-specific spectral bands and Fabry–Pérot interference fringes modulated by strain. These changes correlated linearly with applied deformation ($R^2 > 0.98$). Signal polarity reversed with bending direction, enabling the sensor to distinguish between tensile and compressive strain. To overcome the limitations of peak-intensity-based analysis, 2D correlation spectroscopy was applied to normalised spectral data. The resulting correlation maps revealed distinct, non-linear patterns for each sensor pair. Chemically dissimilar coatings showed low spectral correlation, while similar ones clustered tightly along the diagonal (Fig.2). This method enabled unambiguous segment identification at processing speeds exceeding 300 spectra per second, satisfying the temporal demands of real-time monitoring.

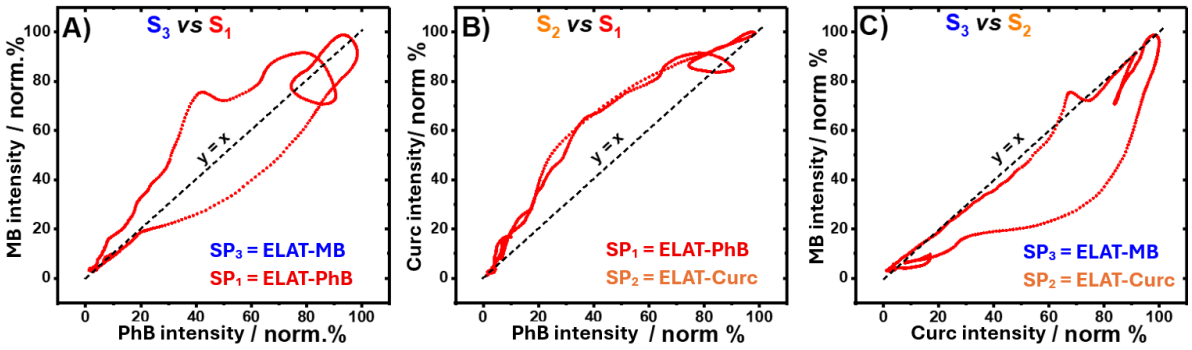

Fig.2 - 2D correlation analysis comparing the spectral signals of sensor-point pairs. (A) ELAT-MB and ELAT-PhB, (B) ELAT-PhB and ELAT-Curc, (C) ELAT-MB and ELAT-Curc.

The tri-point fibre sensor was embedded into a mechanical platform that simulated peristaltic motion through sequential pressure pulses. The spectral data reflected temporally shifted responses across the three sensing sites, enabling accurate reconstruction of propagation dynamics. The ability to resolve localised deformation events in time and space represents a significant improvement over conventional EMG, which often suffers from signal artefacts and limited spatial resolution. [3] The elastomeric coating played a dual role in enhancing both spectral signal strength and structural integrity. The synergy of FEM and 2D COS accelerated the optimisation of the sensor design and enabled deeper insight into the interaction between mechanical strain, fibre geometry, and optical response.

5. Conclusions

In conclusion, the developed anisotropic, surface-modified POF sensor successfully integrates structural design, material functionality and advanced data analysis to enable robust, multipoint biomechanical monitoring. Its application in a peristaltic motion model illustrates its potential for broader use in wearable health technologies, robotic interfaces, and soft prosthetics.

References

[1] L. A. Ngiejungbwen, H. Hamdaoui a M. Chen, „Polymer optical fiber and fiber Bragg grating sensors for biomedical engineering Applications: A comprehensive review,“ *Optics & Laser Technology, vol.* 170, p. 110187, 2024.

[2] E. Korsakova, A. Yuzhakova, D. Salimgareev a e. al., „Mid-infrared silver halide fibre-optic sensor with lateral notches for evanescent wave spectroscopy,“ *Infrared Physics & Technology, vol.* 128, p. 104529, 2023.

[3] M. Al-Ayyad, H. A. Owida, R. Fazio a e. al., „Electromyography Monitoring Systems in Rehabilitation: A Review of Clinical Applications, Wearable Devices and Signal Acquisition Methodologies,“ *Electronics, vol.* 12, p. 1520, 2023.

Innovative composite materials with surface modification, optimized microtopography, thermal conductivity and mechanical properties for the design of artificial tissues and their interfaces

Andrej Tóth[1], Saul Dueñas Casas[1,2], Jerguš Vengríni[1]

[1] *Comenius University, Faculty of Natural Sciences, Department of Physical and Theoretical Chemistry, Ilkovičova 3220/6, 84215 Bratislava, Slovakia*

[2] *University of Matanzas "Camilo Cienfuegos", Department of Chemistry, Carretera a Varadero, Km 3.5, 44740 Matanzas, Cuba*

The presented work focuses on the design, 3D printing and physicochemical characterization of composite materials composed of UV curable photopolymer based on methyl methacrylate filled with hydroxyapatite and pumice with different wt. %. The main objective was to investigate the possibility of fabrication and optimization of the composite material with surface treatments using collagen hydrogel. The work included microscopic and macroscopic modifications of the topology in order to improve the biophysical properties and biocompatibility of the composite. The optimized composite material with the highest tensile strength 47,7 $\pm$ 0,24 MPa (reference value 50 – 150 MPa [1]) contained 70 % (w/w) of transparent photopolymer, 20 % (w/w) of hydroxyapatite and 10 % (w/w) of pumice. The density of this material ($\rho = 1{,}62 \pm 0{,}08\ g \cdot cm^{-3}$) and porosity ($\Phi = 18 \pm 0{,}9\ \%$) average surface roughness ($R_a = 3{,}04 \pm 0{,}15\ \mu m$) are close to the physiological values of cortical bone ($\rho = 2{,}01\ g \cdot cm^{-3}$[1], $\Phi = 15\ \%$ [1]). Average surface roughness of this composite material was $R_a = 3{,}04 \pm 0{,}15\ \mu m$. The thermal conductivity ($0{,}4228 \pm 0{,}021\ W \cdot m^{-1} \cdot K^{-1}$) mimetizing the cortical bone reference value ($0{,}68\ W \cdot m^{-1} \cdot K^{-1}$ [2]) was observed for the combined composite containing 70 % (w/w) photopolymer, 15 % (w/w) hydroxyapatite, and 15 % (w/w) pumice. Thermogravimetric (TGA) analysis confirmed the thermal stability of the composites up to temperatures above 400 °C. The proposed materials and their surface modifications have a significant potential for medical applications.

Keywords: Composite materials, bone implants, gradient interfacing, bio-physical interaction, physicochemical characterization

1. Introduction

The topic of bone implants is an integral part of modern medicine, which aims at continuous optimization and development of new, functionally improved materials with specifically defined physicochemical and mechanical properties. Artificial bone implants are widely used and contribute significantly to improving the quality of life of patients. Their application includes the reconstruction of severe fractures, the insertion of dental implants, as well as the replacement of part or all of the bone tissue due to degenerative, genetic, oncological or other pathological processes [3 – 5].

2. Aims of the study

The aim of the research focuses on the design and characterization of novel inorganic-organic composite materials based on UV-curable methyl methacrylate polymers intended for the development of hard artificial tissues. The surface of the composite materials was modified through the application of collagen hydrogel-containing surface layers. The composite materials and their modified surfaces were subsequently characterized. Their mechanical properties were investigated, and the topology, thermal conductivity, and thermal diffusivity of the newly developed composites were optimized to mimic the characteristics of cortical bone. An interface between soft and hard tissue was designed using a TPMS model.

3. Materials and methods

The following chemicals were used in this work. Distilled water (18,015 g/mol; ddH_2O; 18m Ω/cm), Isopropanol (60,10 g/mol; purity 99,9 %; Centralchem S.R.O., Slovakia), Acetone (58,08 g/mol; P.A; Centralchem S.R.O., Slovakia), butenediol vinyl alcohol copolymer (purity 99,9 %; manufacturer Verbatim, Japan), methyl methacrylate-based rigid photopolymer organic-inorganic composite (TFP, Creality Ltd., China), PremiumFlex flexible photopolymer organic-inorganic composite (EFP, Licquerate GmBH., The Netherlands), pharmaceutical grade synthetic hydroxyapatite (nanoparticles < 200 nm (BET), ≥ 97 % Alfa Aesar), synthetic hydroxyapatite (particles ≤ 100 µm, ≥ 97 %, Merck, USA), synthetic pumice for medical use in the form of microparticles ≤ 300 µm (CENTRITM, UK), Collagen hydrolysate to peptides 200 – 500 Da (Alfa Aesar) enriched up to 15 % with bioactive tripeptides (Gly-Pro-Hyp) and 15 % with bioactive dipeptides (Gly-Pro, Pro- Hyp, Hyp-Gly, 1 : 1 : 1).
FTIR spectra were taken on a Nicolet 6700 spectrometer. XRPD analysis was performed with a URD 6 X-ray diffractometer (Seifert FPM GmbH, Germany) using a copper lamp (λ = 0,154187 nm) and a nickel β-filter, with a step resolution of 0,02° and an exposure time of 1 s/step, at a voltage of 40 kV and a current of 30 mA at room temperature. Transmission spectra and turbidities of the composites were measured with an Agilent 8453 spectrophotometer and a FURKA LAB FIBER spectrometer, respectively. Porosity was measured and calculated using the mercury immersion method. Thermal diffusivity and conductivity were calculated based on experimental data obtained by measuring temperature differences and heat transfer through different thick layers, where a Peltier cell (Type: 12400) and a standard K-probe for temperature measurement (10 measurements /s, ± 0,01°) served as heating element. Testing for resistance to uniaxially applied tension was carried out on the MTS QTest with a strain rate of 2 mm/min. TGA and DTG were performed using a Setaram TGA 92 vertical weighing analysis unit in an argon atmosphere with a dynamic temperature profile at a heating rate of 2 K/min. Printing of butenediol vinyl alcohol copolymer (BVOH) molds was performed on a Prusha i3 MK3S 3D extrusion printer. Curing of the photopolymer composites was performed on an Anycubic Wash & Cure 2.0 machine. The surfaces of the coating composites were observed using a LEICA S8AP0 stereomicroscope with a Flexcam C3 camera at 75x magnification. FEM analysis was

performed by calculation in MATLAB® software, and the calculated intensity values were plotted on the z-axis at individual points on a 500 × 500 point 2D grid.

4. Results

By integrating inorganic particles in the form of hydroxyapatite (HA) and pumice (PE) into an organic-organic UV curable photopolymer composite based on methyl methacrylate with a phosphine oxide photoinitiator (TFP), a change in the topological, mechanical and physicochemical properties of the resulting composite materials was observed. **Fig. 1** shows the variation of porosity [%] and density [g. cm^{-3}] as a function of composite composition.

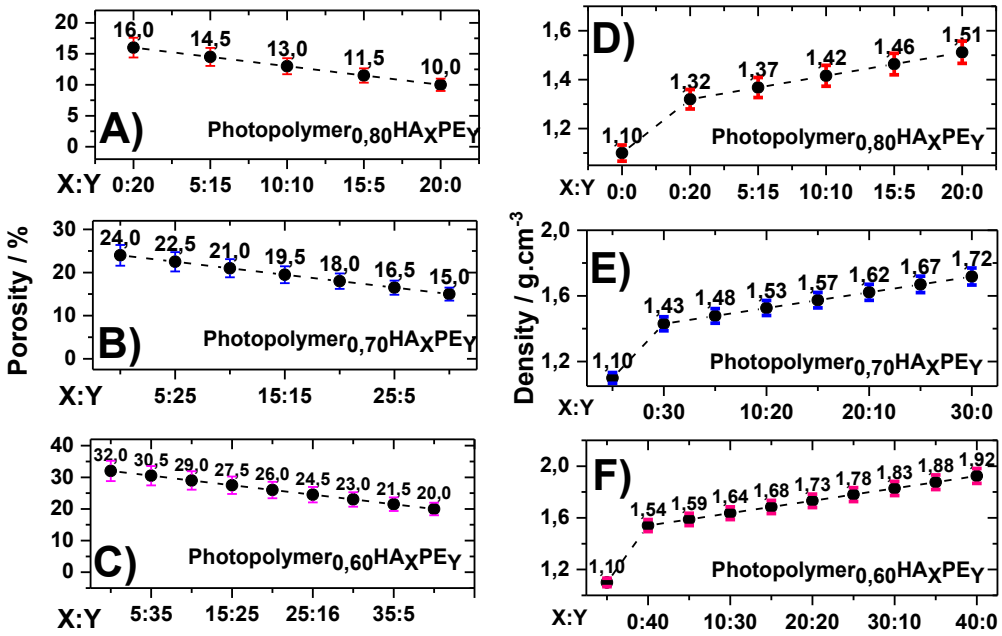

Fig.1 – Porosity of the composites as a function of the ratio of HA and PE microparticles in the sample, within which TFP constituted A) 80 % B) 70 % and C) 60 % of the total weight of the sample, and the change in density as a function of the weight percentage of HA and PE in the sample, within which TFP constituted D) 80 % E) 70 % and F) 60 % of the total weight of the sample. The x-axis describes the individual mass ratios. The first ratio number indicates the HA ratio and the second the PE ratio.

The resulting porosity increased with increasing pumice mass ratio, while the density increased with increasing hydroxyapatite mass ratio. Individual composites exhibiting different compositions also displayed different mechanical properties (**Fig. 2**).

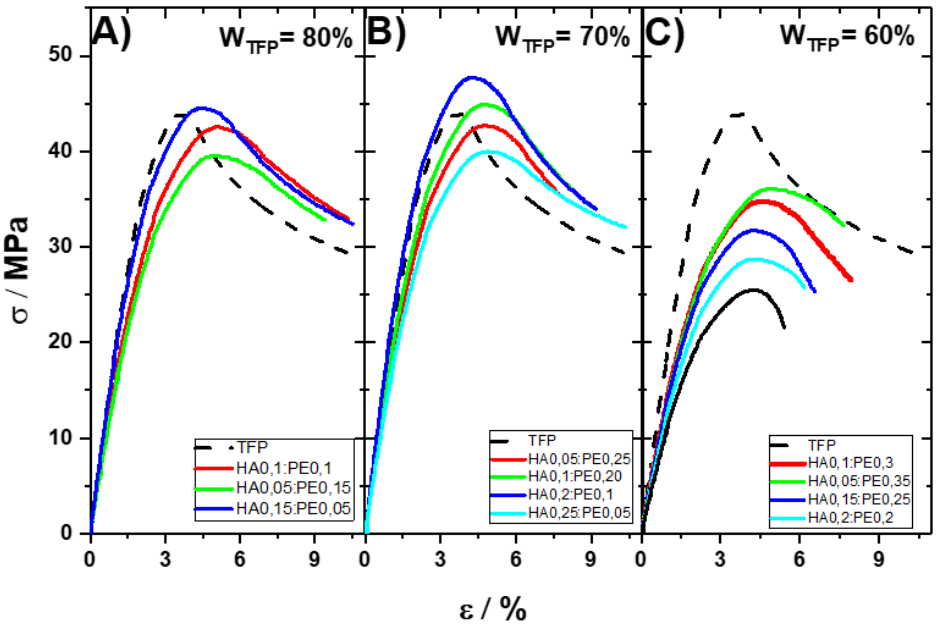

Fig.2 – Stress-strain curves of tensile strength for composite specimens containing 80 % (A), 70 % (B) and 60 % (C) TFP by weight. Different composites contain different ratios of integrated inorganic particles depending on the TFP content.

The highest tensile strength resistance among the three-component composites was recorded for the composite material with a composition of TFP 0,7: HA 0,2: PE 0,1. The thermal diffusivity α and conductivity k for the composite blends with a TFP weight ratio of 70 % is summarized in **Table 1**.

Table 1 - Thermal diffusivities α and thermal conductivities *k* of the prepared composite materials.

Composition	α [$\mathbf{mm^2 \cdot s^{-1}}$]	k [$\mathbf{W \cdot m^{-1} \cdot K^{-1}}$]
TFP	$(5{,}629 \pm 0{,}281) \cdot 10^{-3}$	$2{,}054 \pm 0{,}103$
$TFP_{0,7}HA_{0,3}$	$(3{,}619 \pm 0{,}181) \cdot 10^{-3}$	$0{,}234 \pm 0{,}012$
$TFP_{0,7}$ PE $_{0,3}$	$(4{,}554 \pm 0{,}228) \cdot 10^{-3}$	$0{,}164 \pm 0{,}008$
$TFP_{0,7}$ HAPE $_{0,3}$	$(4{,}053 \pm 0{,}203) \cdot 10^{-3}$	$0{,}423 \pm 0{,}021$
Ref. cortical bone	$1{,}73 \cdot 10^{-1}$ [6]	0,68 [2]

*composite materials are composed of TFP and the corresponding component (HA, PE, HAPE - HA + PE (1:1)

The thermal conductivity of composites containing HA, PE and HAPE is of the order of the reference value of human cortical bone. The thermal diffusivity of the resulting composites differs from the reference value by two orders of magnitude.

5. Conclusion

Among the prepared, studied and characterized inorganic-organic composite materials consisting of integrated inorganic particles in the form of hydroxyapatite and pumice into a UV-curable methyl methacrylate-based photopolymer for potential use as an artificial bone implant, a composite with a composition of TFP 0,7: HA 0,2: PE 0,1 is optimal. This composite exhibited

a tensile strength of 47,7 ± 0,24 MPa, density $\rho = 1{,}62 \pm 0{,}08\ g \cdot cm^{-3}$, porosity $\Phi = 18 \pm 0{,}9$ % mimicking the reference values for human cortical bone. Average surface roughness of this composite material was $R_a = 3{,}04 \pm 0{,}15\ \mu m$.

References

[1] Morgan, E. F., G. U. Unnikrisnan, and A. I. Hussein. 2018. "Bone Mechanical Properties in Healthy and Diseased States." *Annual Review of Biomedical Engineering* 20 (1): 119–143. https://doi.org/10.1146/annurev-bioeng-062117-121139.

[2] Feldmann, A., P. Wili, G. Maquer, and P. Zysset. 2018. "The Thermal Conductivity of Cortical and Cancellous Bone." *European Cells and Materials* 35: 25–33. https://doi.org/10.22203/eCM.v035a03.

[3] Lichte, P., H. C. Pape, T. Pufe, P. Kobbe, and H. Fischer. 2011. "Scaffolds for Bone Healing: Concepts, Materials and Evidence." *Injury* 42 (6): 569–573. https://doi.org/10.1016/j.injury.2011.03.033.

[4] Bose, S., M. Roy, and A. Bandyopadhyay. 2012. "Recent Advances in Bone Tissue Engineering Scaffolds." *Trends in Biotechnology* 30 (10): 546–554. https://doi.org/10.1016/j.tibtech.2012.07.005.

[5] Myeroff, C., and M. Archdeacon. 2011. "Autogenous Bone Graft: Donor Sites and Techniques." *Journal of Bone and Joint Surgery* 93 (23): 2227–2236. https://doi.org/10.2106/JBJS.J.01513.

[6] Zhang, Y., M. Gan, and V. Tomar. 2019. "Nanomechanical Raman Spectroscopy in Biological Materials." In *Encyclopedia of Biomedical Engineering*, 215–228. https://doi.org/10.1016/B978-0-12-801238-3.99917-3.

Study of Composite Conductive Layers Based on Graphite and Doped ZnO Nanoparticles For Sensor Integration into 3D-Printed Cardiac Valves and Vascular Structures

Viktória Pohorelská[1], Mária Martinická [1] , Samuel Furka [1]

[1] *Comenius University, Faculty of Natural Sciences, Department of Physical and Theoretical Chemistry, Mlynska dolina, Ilkovičova 6, 841 04 Bratislava Slovakia*

The integration of smart materials into artificial tissues represents a key advancement in biomedical engineering. Materials capable of detecting mechanical load and structural degradation through changes in their electrical properties that offers a promising route toward autonomous implant monitoring. In cardiovascular applications, continuous mechanical loading presents a significant challenge to implant longevity. In this study we studied a composite sensor system based on vinyl-acetate matrix mixed with graphite, starch granules and ZnO nanoparticles—both pure and doped with Al^{3+}, Fe^{3+} and B^{3+} ions.

ZnO is wide-bandgap semiconductor with value of 3.37 eV known for its high chemical stability, piezoelectricity and biocompatibility, making it suitable for applications in biosensors [1]. Its electrical and structural properties can be precisely tuned through doping. Hydrothermal synthesis was used to obtain pure and doped ZnO nanoparticles, ensuring its high crystallinity and morphological control under specific conditions.

References:

[1] Y. Zhang, T. R. Nayak, H. Hong, and W. Cai, “Biomedical Applications of Zinc Oxide Nanomaterials,” *Curr Mol Med*, vol. 13, no. 10, p. 1633, Dec. 2013, doi: 10.2174/15665240136661311111130058.

1. Introduction

The development of intelligent cardiovascular implants represents a growing interdisciplinary challenge that connects material science, physical chemistry, nanotechnology and medicine. Implants, particularly vascular grafts and cardiac valves are constantly subjected to cyclic mechanical loading, making real-time sensing of microtears a critical functionality.[2] Exploring the possibility of preparing an inorganic-organic composite layer with adjustable

electrical conductivity, frequency dependent capacitive reactance and impedance can be intended for integration into artificial 3D printed blood vessels, as a sensor responsive to the changes under cyclic mechanical overload over time.

In this context, composite materials combining organic polymer matrixes with functional fillers offer a promising approach. ZnO nanoparticles stand out for their high chemical stability, wide band gap (E_g≈3,37 eV) and strong exciton binding energy (≈60 meV) make them a suitable candidate for use in sensorics layers [1].

2. Materials and Methods

2.1 Compounds evaluated

Zinc acetate dihydrate ($Zn(Ac)_2 . 2H_2O$, > 98.5%), boric acid (H_3BO_3, 99,9%), iron(III) nitrate nonahydrate ($Fe(NO_3)_3 . 9H_2O$, > 99,9 %, CAS: 7782-61-8) and aluminium nitrate nonahydrate ($Al(NO_3)_3 . 9H_2O$, > 99,9 %) were used for the synthesis of pure and doped nanoparticles, were purchased from Alfa Aesar, Germany. Graphite powder (< 100 µm, ≥ 98%) was obtained from KOH-I-NOOR Hardtmuth GmbH., Austria. Vinylacetate (CAS: 108-05-4) and 2,2-dibromo-2-cyanoacetamide (CAS: 10222-01-2) were purchased from Merck, USA. Sodium bicarbonate ($NaHCO_3$, > 99,9 %) was also supplied by Alfa Aesar, Germany, 26 % aqueous ammonia solution was obtained from Mikrochem s.r.o, Slovakia. Ultrapure distilled deionized water H_2O (18.2 MΩ/cm pri 297 K) was prepared by reverse osmosis. Organic solvents acetone, methanol, ethanol and isopropanol were purchased from Central Chem s.r.o, Slovakia, all with a purity of 99,5 %. As the elastic printing material based on urethane-methyl methacrylate we used Premium Flex® from Licquerate, Netherlands.

2.1 Methods

ZnO nanoparticles were synthetized using hydrothermal synthesis using zinc acetate as the precursors. Dopants were introduced at a 10 mol% ratio by co-precipitation with $Al(NO_3)_3$, $Fe(NO_3)_3$ and H_3BO_3. The crystallinity was confirmed by powder X-ray diffraction (PXRD) revealing the hexagonal wurtzite structure with successful dopant incorporation. Fourier-transform infrared spectroscopy (FTIR) was used to confirm ZnO bonding and to assess the chemical integrity of materials. Composites were prepared by dispersing synthetized nanoparticles with graphite and starch into a vinyl acetate matrix. The graphite was used to create conductive phase and starch granules were used to promote stress sensitivity. Electrical

characterization was performed using an LCR meter in the 100 Hz – 10 kHz range to measure frequency-dependent impedance and capacitive reactance.

3. Results

We analyzed the percolation threshold of every compound. Electrical analysis revealed a percolation threshold between 10% and 15% (w/w) graphite, starch and ZnO nanoparticles. Structural changes of the material were reflected in the impedance spectra of the materials. Fig.1 shows dependence of concentration of fillers on frequency-independent and frequency-dependent electrical properties.

The composite containing 15% (w/w) graphite, 20% (w/w) starch and 10% Al-doped ZnO nanoparticles showed the most favorable frequency-dependent electrical characteristics. This variant showed stable impedance responses under cyclic mechanical conditions. Fig.2 represents effect of the number of bending cycles on frequency-independent resistance, frequency-dependent capacitance and impedance of the ZnOAl (10%) composite measured at a frequency of 120Hz.

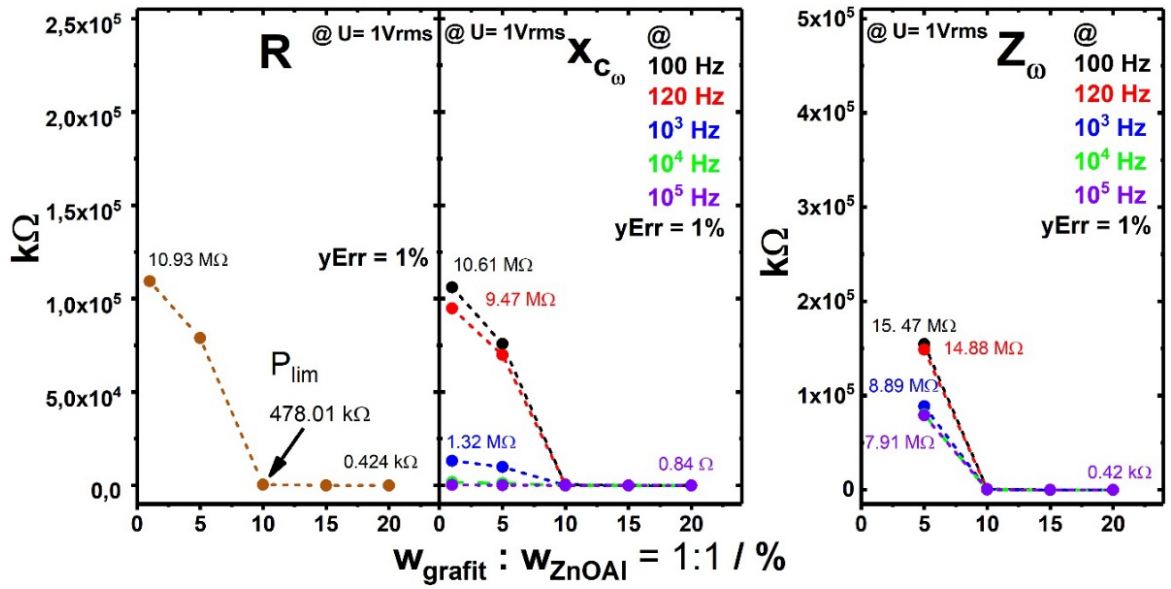

Figure 1.: Dependence of concentration of graphite and Al-doped ZnO nanoparticles on frequency-independent conductivity (R), frequency-dependent capacitance (X_c) and impedance (Z) of a material with vinyl-acetate matrix

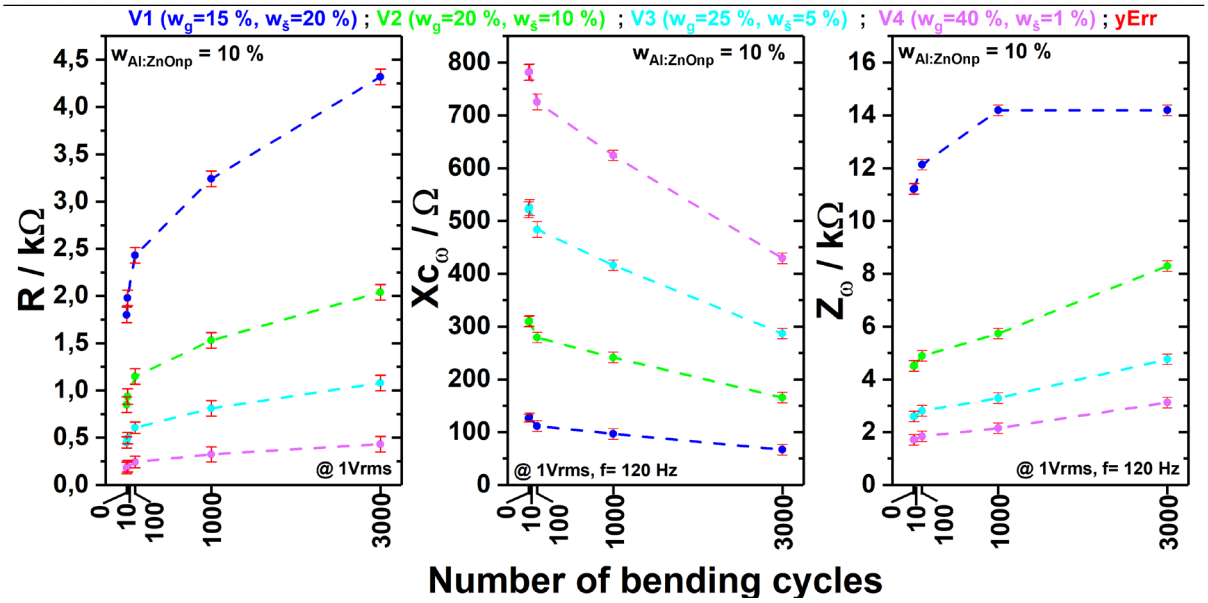

Figure 2.: Effect of the number of bending cycles on frequency-independent resistance, frequency-dependent capacitance and impedance of the ZnOAl (10%) composites measured at a frequency of 120Hz.

4. Discussion

The electrical parameters of the prepared composite, particularly their percolation limit, reflects the interconnection between filler, vinyl-acetate matrix and induced microdamage. Doping with ZnO with Al^{3+}, Fe^{3+} and B^{3+} altered the electrical properties of the composites. Among tested dopants, aluminum-doped ZnO (10 mol%) exhibited the most favorable impact on impedance characteristics, suggesting enhanced charge mobility. PXDR and FTIR analyses confirmed the successful incorporation of dopants into the wurtzite crystal structure, which likely contributed to the observed improvements of electrical parameters. Starch promoted localized stress concentration, leading to the formation of microcracks during cyclic bending.

These structural disruptions resulted in detectable shifts in frequency-independent and frequency-dependent electrical parameters, particularly at lower frequencies (e.g. 120Hz). The correlation between mechanical fatigue and electrical response supports the use of such a system in health monitoring.

The composite containing 15% graphite, 20% starch, and 10% Al-doped ZnO demonstrated the most pronounced and consistent frequency-dependent electrical changes across repeated bending cycles. The cured 3D-printed structure was then surface-modified with this functional sensory layer based on a vinyl acetate composite. Before drying, impedance measurement electrodes were integrated at a 3 cm distance from each other. After drying, a thin protective layer of Premium Flex photopolymer was applied and cured over the surface to

isolate the sensory layer from the external environment, minimizing interference in its electrical properties.

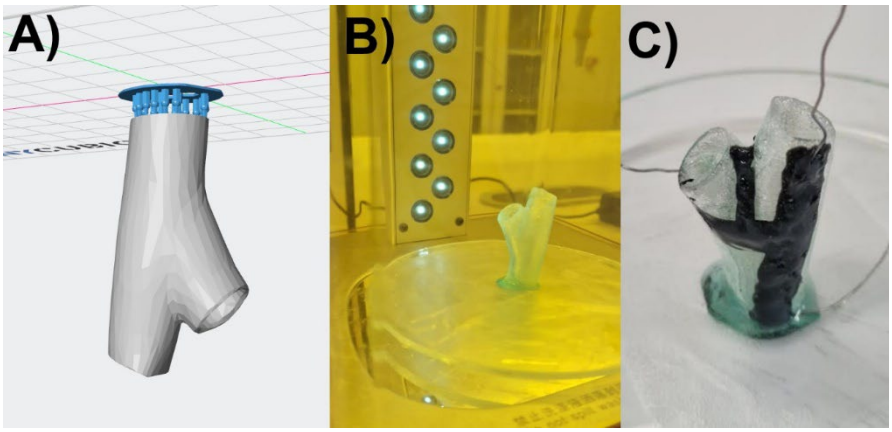

Figure 3. – Optimized 3D model of the left pulmonary vessel: (A) prepared for 3D printing from elastic photopolymer Premium Flex using AnycubicPhotonWorkshop 3.6.2; (B) post-processing curing; (C) printed model with surface treatment using a (black) composite sensory layer with integrated electrodes.

This behaviour positions the material as a viable candidate for a sensor layer in biomedical applications, specifically on the surface of 3D-printed vascular grafts. Notably, the presence of starch increased the composite's sensitivity to fatigue-induced damage without compromising the structural integrity required for implant integration.

5. Conclusions

Composite demonstrates the successful design and contains suitable for sensor integration into vascular and cardiac implants. A specific composition, including graphite, starch and aluminium-doped ZnO nanoparticles, offered optimal performance. The developed system enables non-invasive monitoring of mechanical stress through analysis of electrical properties, offering potential application in smart implants capable of detecting early mechanical failure.

References

[1] Y. Zhang, T. R. Nayak, H. Hong, and W. Cai, "Biomedical Applications of Zinc Oxide Nanomaterials," *Curr Mol Med*, vol. 13, no. 10, p. 1633, Dec. 2013, doi: 10.2174/15665240136661311111130058.

[2] S. Mitragotri and J. Lahann, "Physical approaches to biomaterial design," *Nat Mater*, vol. 8, no. 1, pp. 15–23, 2009, doi: 10.1038/nmat2344.

Biochemical Diagnosis of Congenital Adrenal Hyperplasia Using Mass Spectrometry-Based Methods

Andrej Bandura[a],

[a] Comenius University, Faculty of Medicine, Institute of Medical Biology, Genetics and Clinical Genetics, Sasinkova 4, 811 08, Bratislava, Slovakia

Abstract

Steroid compounds are biologically active molecules that play a crucial role in the regulation of a wide range of cellular processes. The synthesis of steroid compounds can be influenced by genetic disorders affecting the enzymes involved in their production and degradation. These disorders typically affect endocrine glands (adrenal glands and gonads) and tissues containing target receptors, leading to significant metabolic imbalances. Determination of steroid concentrations in body fluids is essential for the diagnosis of pathological conditions, including endocrine disorders and inherited metabolic diseases, which are often characterized by abnormal hormone levels. Over the past decades, methodological approaches have evolved significantly, with improvements in specificity and sensitivity. Mass spectrometry-based methods have come to the forefront as the most reliable techniques for meeting these criteria.

Keywords: congenital adrenal hyperplasia, serum, urine, chromatography, mass spectrometry

Introduction

Congenital adrenal hyperplasia (CAH) is a group of disorders characterized by a deficiency of one of the enzymes involved in steroidogenesis. Impaired cortisol synthesis leads to a feedback-driven increase in adrenocorticotropic hormone (ACTH) secretion, resulting in subsequent adrenal cortex hyperplasia. This process causes the accumulation of certain steroid hormone precursors and a metabolic shift toward excessive androgen production (1,2). The biosynthetic pathways of steroid production are interconnected. Steroid synthesis occurs in morphologically and enzymatically distinct zones of the adrenal cortex, which produce three types of steroid hormones: mineralocorticoids (zona glomerulosa), glucocorticoids (zona fasciculata), and androgens (zona reticularis) (3).

Deficiency or reduced activity of 21-hydroxylase (CYP21) is the most common form of CAH, accounting for more than 90% of cases. The continuous spectrum of enzymatic activity in 21-hydroxylase deficiency leads to varying severity of clinical manifestations. The most severe form, characterized by a complete absence of glucocorticoids and mineralocorticoids, represents the classic salt-wasting form of CAH. The resulting increase in androgen production causes prenatal masculinization with ambiguous genitalia in females and postnatal virilization in both sexes (4). A life-threatening salt-wasting crisis may occur, accompanied by severe metabolic disturbances and cerebral edema. In the simple virilizing form, partial 21-hydroxylase deficiency leads to prenatal masculinization in females and postnatal virilization in both sexes, but without significant impairment of salt metabolism. The mildest, non-classic, late-onset form manifests clinically in adulthood, presenting as polycystic ovary syndrome, menstrual irregularities, and hirsutism in women, and infertility due to androgen excess in men (5).

Deficiency of 11β-hydroxylase (CYP11B1) is the second most common form of CAH, accounting for approximately 5% of cases. 11β-hydroxylase deficiency leads to accumulation of 11-deoxycorticosterone, a hormonally weaker precursor of aldosterone, which typically results in hypertension. The androgen pathway is not impaired by this enzyme deficiency; instead, a shift in steroidogenesis toward androgen overproduction causes clinical features similar to those seen in 21-hydroxylase deficiency (5), prenatal masculinization occurs in females, and postnatal virilization is observed in both sexes (6).

Materials and Methods

In cases of clinical suspicion of CAH, diagnostic evaluation is based on two complementary approaches: 1.) a molecular genetic approach aimed at precise identification of gene variants (mutations) and assessment of their pathogenicity through comparison with reference databases; and 2.) biochemical approach based on the analysis of selected steroid hormones, their metabolites, precursors, and precursor metabolites (biomarkers). Hormone precursors and their metabolites appear in plasma, and when a biosynthetic block is present, they accumulate in significant quantities and undergo further metabolic conversions. This results in a broad spectrum of metabolites that are subsequently eliminated in urine and bile, which can provide a rich source of diagnostic information. From the perspective of expert diagnostics, accurate determination of the spectrum and quantity of steroid compounds in body fluids is essential.

Based on the known pathways of steroidogenesis (Scheme 1) and steroid biotransformation (Scheme 2), as well as published literature, several metabolites were selected as potential biomarkers for specific forms of CAH (7–10). **In 21-hydroxylase deficiency**, 17-hydroxyprogesterone accumulates upstream of the enzymatic block and is included in newborn screening programs, which are currently performed from dried blood spots using immunoassays, despite their known limitations (11,12). Serum 21-deoxycortisol serves as a more specific biomarker, with elevated levels being pathognomonic for this form of CAH. In urine, elevated excretion of pregnanetriol (PT), 17-hydroxypregnanolone (17HP), and pregnanetriolone (PTONE) is characteristic of 21-hydroxylase deficiency (13). Urinary metabolites are analyzed by GC-MS, while serum steroids are quantified by LC-MS/MS. It may be advantageous to determine a diagnostic ratio of selected metabolites, e.g., PTONE:THE, or (17HP + PT):(THE + THF + 5αTHF) (14). In **11β-hydroxylase deficiency**, the accumulating metabolites are 11-deoxycorticosterone (DOC) in the mineralocorticoid synthetic pathway and 11-deoxycortisol (S) in the glucocorticoid pathway (14). Diagnosis based on urinary metabolites relies on ratios such as THS:(THE + THF + 5αTHF) (14), (androsterone + etiocholanolone):(THE + THF + 5αTHF) (11). Elevated tetrahydro-11-deoxycortisol (THS) has a high positive predictive value.

The aim was to identify suitable biomarkers, ESI spectra of selected standards, optimize chromatographic separation, MS detection parameters, and sample pretreatment protocols, given that the analytes are present in complex biological matrices at trace concentrations.

The samples consisted of serum, routinely obtained by collecting blood into tubes without anticoagulant followed by centrifugation (or plasma in tubes containing anticoagulant)

and urine obtain to urine tubes. The chemicals and laboratory materials used included: methanol (Honeywell, CHROMASOLV, gradient grade), acetonitrile (Supelco, LiChrosolv, gradient grade), methyl tert-butyl ether (Sigma-Aldrich, ACS reagent), deionized water, formic acid (Merck, for HPLC), acetic acid (Merck, for HPLC), 17α-hydroxyprogesterone (Sigma-Aldrich, ≥95%), pregnantriol (Sigma-Aldrich, ≥95%), 17α-hydroxyprogesterone-d8 (2,2,4,6,6,21,21,21-d8, Cerilliant, 100 µg/mL in methanol, certified reference material), Discovery DSC-18 SPE tubes (Supelco, 500 mg sorbent, 6 mL tube volume), Merck RP-18 (Merck, 200 mg sorbent, 3 mL tube volume), HybridSPE Phospholipid Ultra Cartridge (Supelco, 30 mg sorbent, 1 mL tube volume), Strata-X Polymeric RP (Phenomenex, 200 mg sorbent, 3 mL tube volume), and other standard laboratory equipment (microtiter plates, vials, automatic pipettes, pipette tips, Hamilton microsyringe, Eppendorf tubes of various sizes, centrifuge, and heating shaker.

Chromatographic analysis was performed using a Surveyor LC Pump Plus system (Thermo) coupled with a Finnigan Surveyor Autosampler Plus and a TSQ Quantum GC mass spectrometer (Thermo Scientific) equipped with a HESI-II ionization source operating at atmospheric pressure. Thermo XCalibur software was used for instrument control and data evaluation. Quantification was carried out in Selected Reaction Monitoring (SRM) mode.

For separation was used ZORBAX RR StableBond C18 column (2.1 mm i.d. × 150 mm length, 3.5 µm particle size; Agilent Technologies, 830990-902). The column temperature was maintained at 35 °C. The mobile phase flow rate was set to 300 µL/min. Gradient elution was performed using the following mobile phases: mobile phase A – methanol; mobile phase B – water; mobile phase C – methanol with 1% formic acid. The gradient started from a 50:50 water-to-organic ratio and progressed to 100% organic phase, followed by re-equilibration to the initial conditions. The HESI-II ion source was operated in positive ion mode with a spray voltage of 4500 V and a vaporizer temperature of 350 °C. Nitrogen (N_2) was used as the nebulizing and drying gas: sheath gas pressure 35 AU, sweep gas pressure 1.0 AU, and auxiliary gas pressure 20 AU. The transfer capillary temperature was set to 350 °C. The mass spectrometer operated in SRM mode with a collision cell gas pressure of 1 mTorr using argon as the collision gas. The monitored precursor-to-product ion transitions were 331.4 → 97.3; 109.3 for 17-hydroxyprogesterone and 339.4 → 100.3; 113.2 for d_8-17-hydroxyprogesterone.

Sample pretreatment protocols: Liquid-liquid extraction (LLE) was performed using methyl tert-butyl ether (MTBE). Solid-phase extraction (SPE) was tested with several sorbents: C18 bonded to a silica support, a styrene-divinylbenzene polymer (Strata-X), and a zirconia-modified silica sorbent for phospholipid removal. In general, the sample preparation procedure involved protein precipitation with acetonitrile followed by centrifugation (10,000 rpm). The supernatant was diluted with water to reduce the organic solvent content and then subjected to SPE (or extracted with MTBE in the case of LLE). Each SPE cartridge was conditioned prior to loading the diluted supernatant, washed to remove polar compounds, and subsequently eluted with methanol or an alternative elution solvent. The eluate was dried to completeness under a stream of air while shaking on a heated shaker at 50 °C. The dried extracts were reconstituted in 50% methanol containing 0.05% formic acid and prepared for HPLC-MS/MS analysis.

Results

MS/MS parameters for 17-hydroxyprogesterone and d8-17-hydroxyprogesterone were obtained using TSQ Tune software. The maxima of the tuning curves corresponded to the optimal collision energy for the selected transitions.

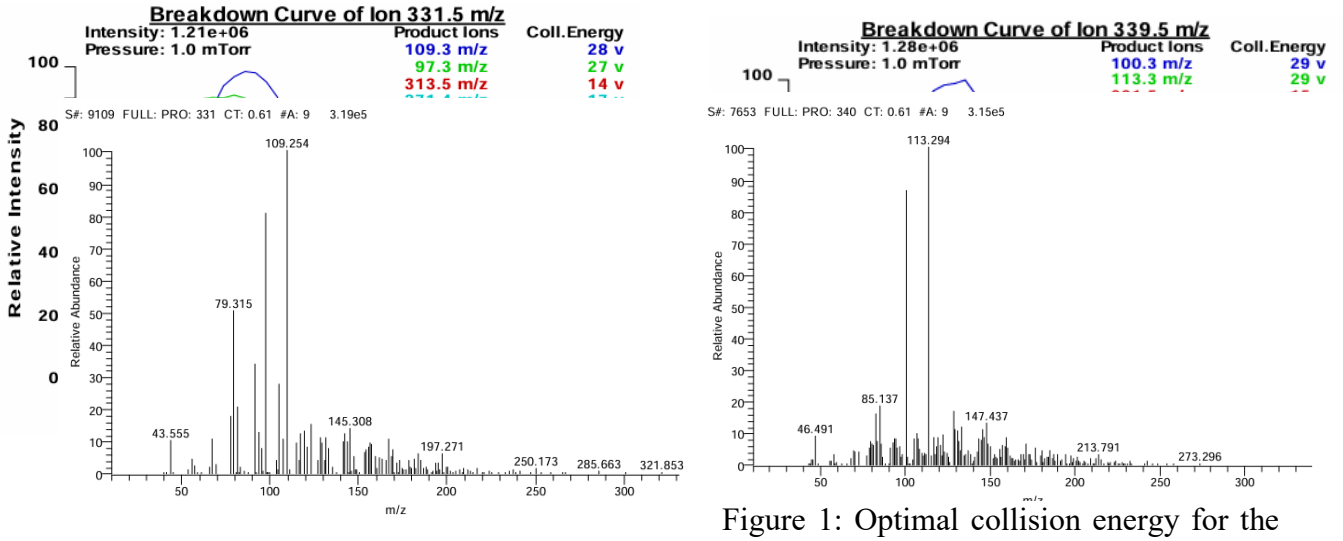

Figure 1: Optimal collision energy for the precursor ion $[M+H]^+$ m/z 331.4 corresponding to 17OHP and for $[M+H]^+$ m/z 339,5; corresponding to d8 17OHP.

Figure 2: Mass spectra in MS2 quadrupole after CID, corresponding to 17OHP and to d8 17OHP respectively.

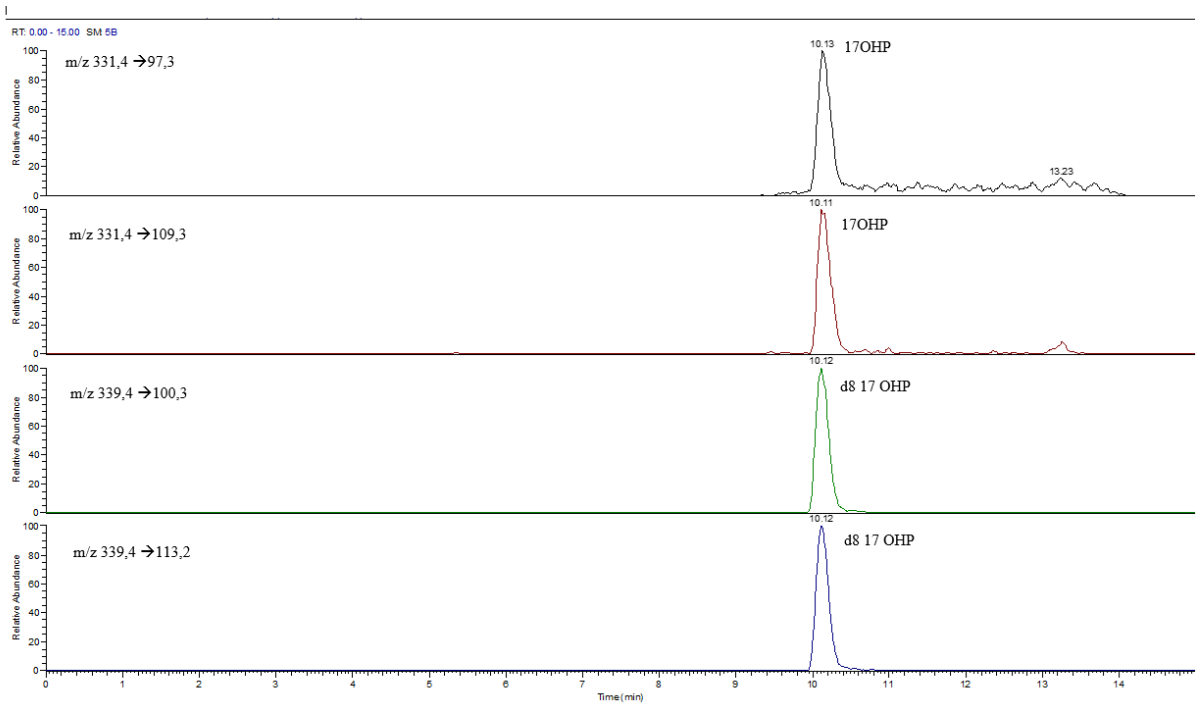

Figure 3: HPLC-MS/MS chromatogram showing the separation of 17OHP at a concentration level of 5 µg/L and the internal standard d_8-17OHP at 18.75 µg/L in solvent.

Sample pretreatment protocols results displayed in Figure 4. The overall efficiency of the sample preparation process reflects both extraction recovery and matrix effects (ion suppresion in ESI). The highest efficiencies were achieved by combining HybridSPE for phospholipid removal with subsequent extraction on Strata-X cartridges. Acceptable results were also obtained using HybridSPE alone, due to the simplicity of the procedure. For HybridSPE, a maximum serum volume of 100 µL could be processed, determined by the sorbent mass and cartridge volume, which affected the final concentration (or dilution) of the sample. It would be advisable to use cartridges compatible with larger serum volumes.

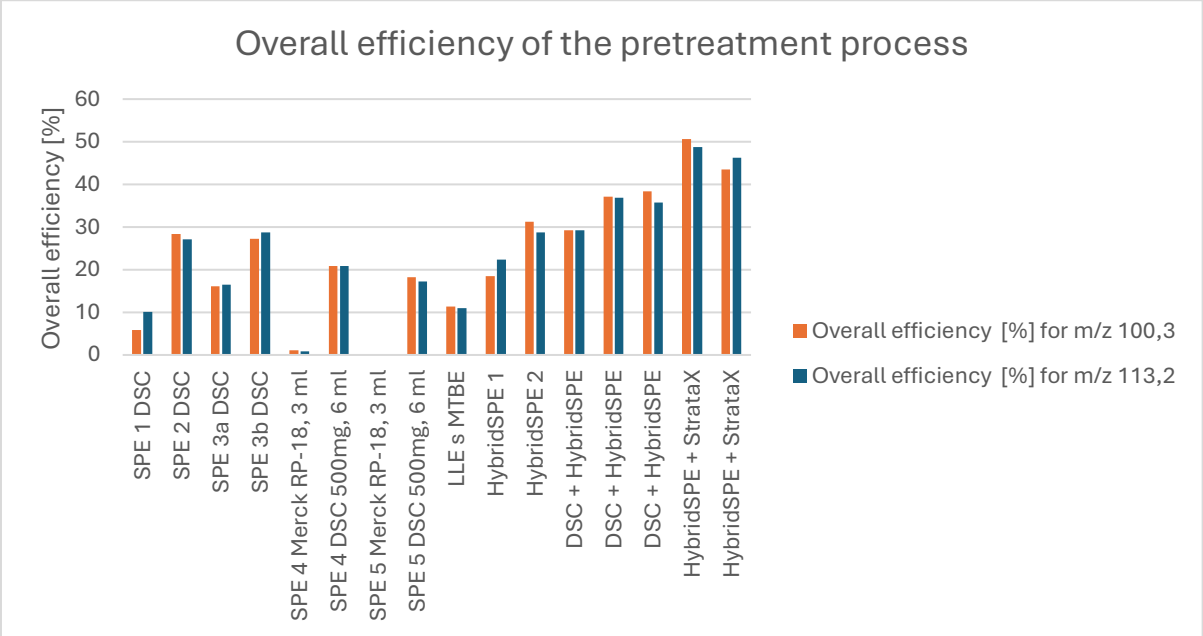

Figure 4: Overall efficiency of the pretreatment process. Each pair of columns (obtained for the qualifier and quantifier MS/MS transitions) corresponds to the overall efficiency after modification of the sample pretreatment procedure. In liquid-liquid extraction, an efficiency of approximately 10% was observed, likely due to strong matrix effects, while solid-phase extraction proved to be more efficient. The higher overall efficiency observed in experiments with HybridSPE reflects reduced matrix effects, as the final concentration factor was lower.

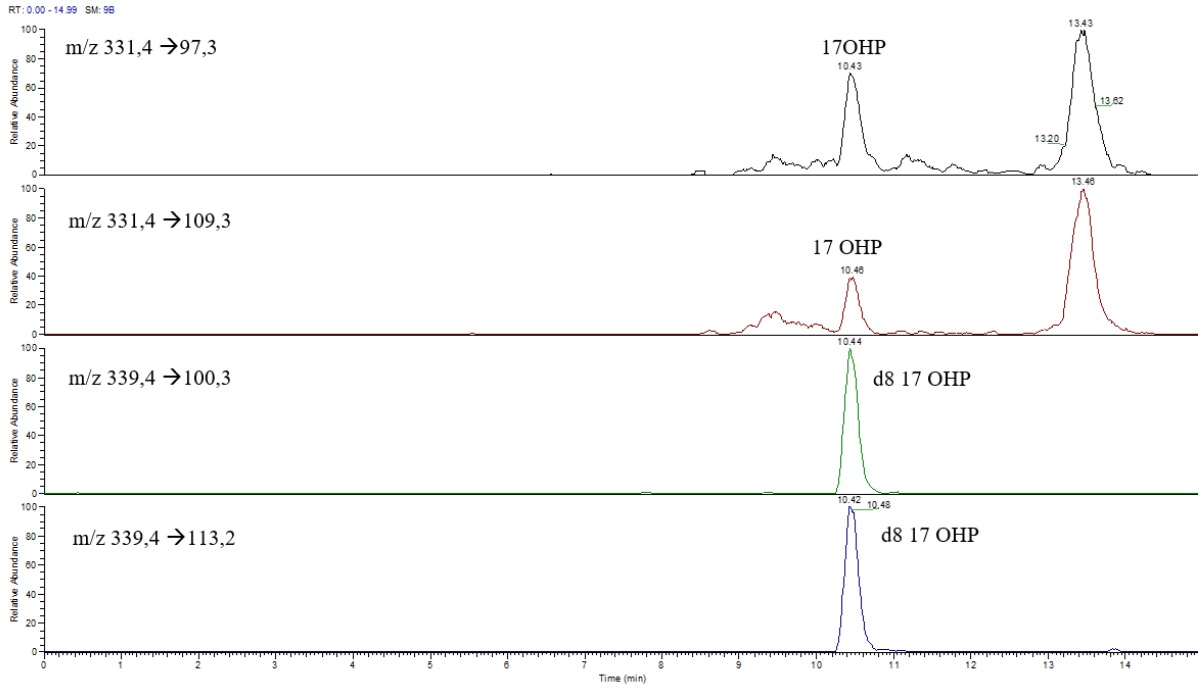

Figure 5: A chromatogram showing the separation of a serum sample spiked, prepared using the HybridSPE 2 procedure at a concentration level of 6 µg/L for 17OHP and 18.75 µg/L for d_8-17OHP.

Results obtained with standard addition method:

With normalization to ISTD peak areas for m/z 97.3/100.3: **0.66 µg/l,** peak areas for m/z 109.3/113.2: **0.75 µg/l**

Results obtained with one-point calibration method:

peak areas for m/z 97.3/100.3: **0,75 µg/l,** peak areas for m/z 109.3/113.2: **0,98 µg/l**

Conclusion

As the samples consisted of serum without suspected steroidogenesis disorders, the expected concentrations were within the physiological range, which was consistent with the results obtained. Given that the analyte is present in positive samples at 10- to 100-fold higher concentrations and after optimization of the sample preparation process, chromatographic separation, and MS detection, the method is considered suitable for the diagnosis of CAH due to 21-hydroxylase deficiency. The current approach can serve as a basis for further development and optimization of the method for clinical application. It is desirable to expand the panel to include additional metabolites with similar approach and pretreatment technique, enabling the diagnosis of rarer forms of CAH. With the increasing volume of data in the form of chromatograms, mass spectra, and quantified laboratory results, the importance of proper data analysis has become especially relevant and essential

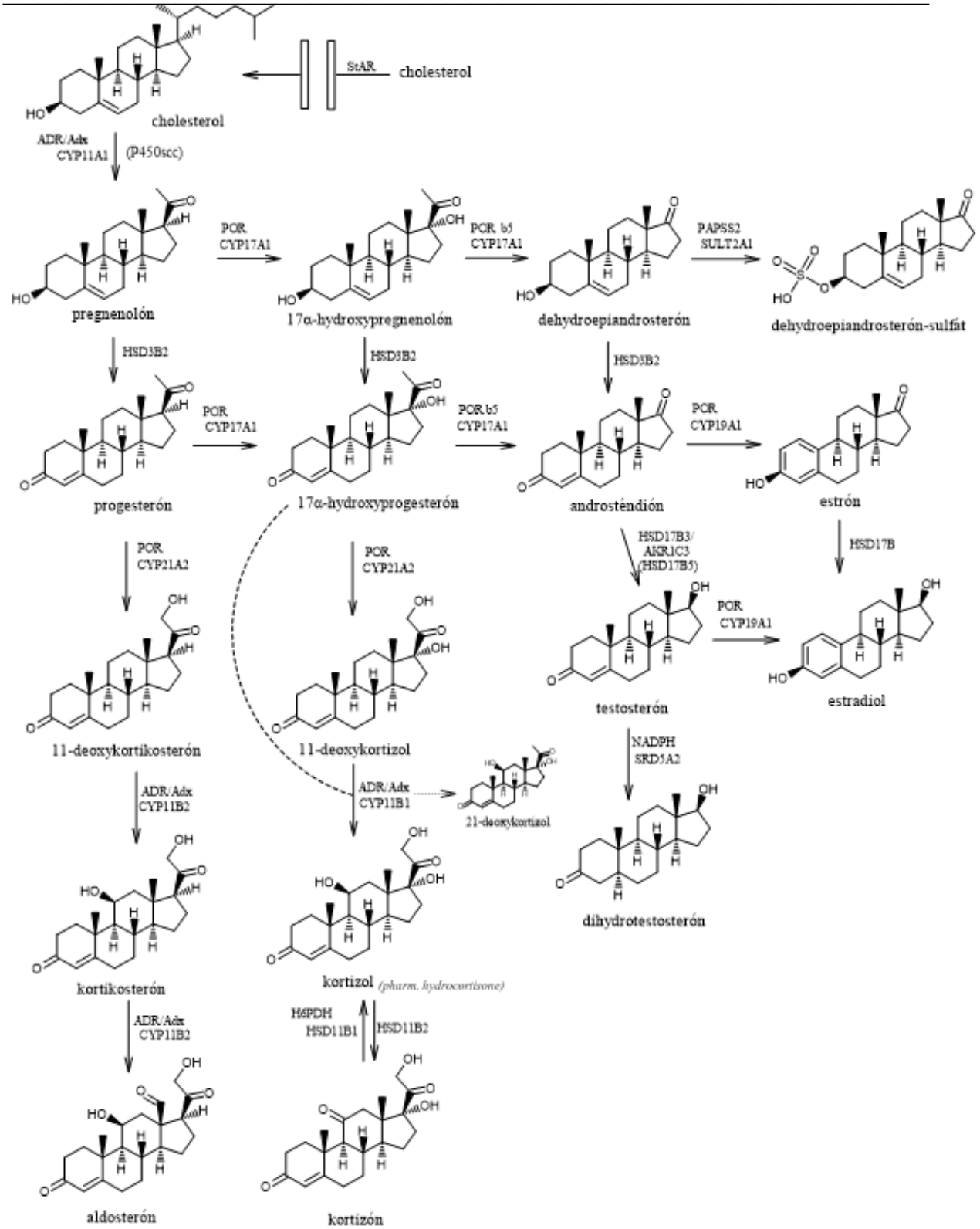

Scheme 1 - Steroidogenesis

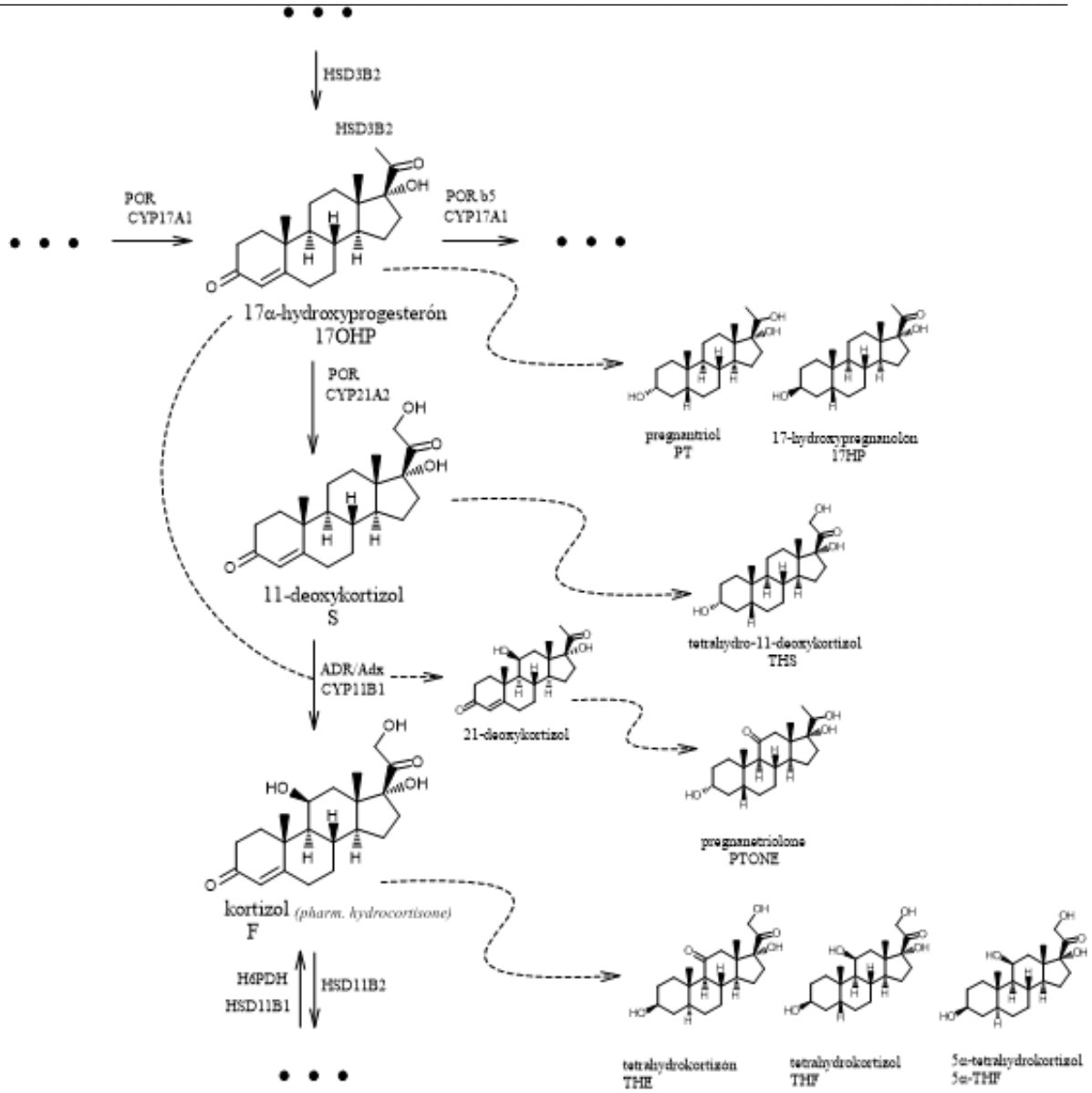

Scheme 2 – Steroid biotransformation reactions

References

1. Muntau A. Intensivkurs Pädiatrie. 6. Auflage. München: Elsevier, Urban & Fischer; 2011. 574 p.
2. Sadler TW. Langman's medical embryology. 13th edition. Philadelphia: Wolters Kluwer; 2015. 407 p.
3. Kapeller K, Pospíšilová V. Embryológia človeka: učebnica pre lekárske fakulty. 2. vydanie. Osveta; 2001. 370 p.
4. El-Maouche D, Arlt W, Merke DP. Congenital adrenal hyperplasia. Lancet Lond Engl. 2017 Nov 11;390(10108):2194–210.
5. Pastoráková A, Petrovič R, Pribilincová Z, Knapková M, Malová J, Varchulová Nováková Z, et al. Molekulovogenetická podstata a diagnostika kongenitálnej adrenálnej hyperplázie na Slovensku. Lekársky obzor. 2020;s. 112-121.
6. Scriver CR, Sly WS, Childs B, Beaudet AL, Valle D, Kinzler KW, et al. The Metabolic and Molecular Bases of Inherited Disease, 4 volume set. 8th edition. New York: McGraw-Hill Professional; 2000. 6338 p.

7. Guo T, Chan M, Soldin SJ. Steroid profiles using liquid chromatography-tandem mass spectrometry with atmospheric pressure photoionization source. Arch Pathol Lab Med. 2004 Apr;128(4):469–75.
8. Kushnir MM, Rockwood AL, Roberts WL, Pattison EG, Bunker AM, Fitzgerald RL, et al. Performance characteristics of a novel tandem mass spectrometry assay for serum testosterone. Clin Chem. 2006 Jan;52(1):120–8.
9. van der Veen A, van Faassen M, de Jong WHA, van Beek AP, Dijck-Brouwer DAJ, Kema IP. Development and validation of a LC-MS/MS method for the establishment of reference intervals and biological variation for five plasma steroid hormones. Clin Biochem. 2019 Jun;68:15–23.
10. Šimková M, Kolátorová L, Drašar P, Vítků J. An LC-MS/MS method for the simultaneous quantification of 32 steroids in human plasma. J Chromatogr B. 2022 Jun 30;1201–1202:123294.
11. Blau N, Duran M, Gibson KM, editors. Laboratory guide to the methods in biochemical genetics. Berlin: Springer; 2008. 860 p.
12. Lysinová M, Knapková M, Dluholucký S, Králinský K. Novorodenecký skríning v súčasnosti. Pediatr Prax. 2015;(16):188–91.
13. Shackleton CH. Mass spectrometry: application to steroid and peptide research. Endocr Rev. 1985;6(3):441–86.
14. Kamrath C, Wudy SA, Krone N. Steroid biochemistry. Endocr Dev. 2014;27:41–52.


BLOK II:
DÁTA,
ALGORITMY,
ROZHODNUTIA:
AI
AI A ANALYTIKA
V SLUŽBÁCH
BIOMEDICÍNY

AI-Assisted Profiling of multidimensional data for Gut Phenotype Classification: Development and Validation of the QUANTUM Diagnostic Platform.

Daniel Furka [1], Samuel Furka [1], Martin, Haranta [2], Norbert Bomba [2]

[1] *Comenius University, Faculty of Natural Sciences, Department of Physical and Theoretical Chemistry, Ilkovičova 3220/6, 84215 Bratislava, Slovakia*
[2] *PerBiotiX s.r.o., Palárikova 2657 022 01 Čadca, Slovakia*

Recent advances in artificial intelligence (AI), machine learning, and multidimensional statistical analysis have significantly transformed the field of metabolomic diagnostics. These technologies enable high-throughput evaluation of complex biological matrices without extensive sample preprocessing or compound-specific separation. The QUANTUM analyser platform, developed over fourteen years of interdisciplinary research, integrates AI-based data processing with physicochemical sensor technologies to generate disease-relevant diagnostic profiles called “fingerprints” from stool, urine, and other biofluids. This platform has demonstrated fingerprint-matching accuracy up to 82 percent for specific diseases, with false positive rates ranging from 10 to 17 percent. It is capable of identifying gut phenotypes, microbial imbalances, and pathological patterns through data-driven clustering and signal interpretation. By analysing multidimensional signal profiles, the system distinguishes seven core gut phenotypes and maps 26 disease-associated subclusters. The QUANTUM technology is currently being applied in clinical and field studies across Slovakia, Kenya, and Canada. Its portability, reagent-free operation, and rapid analytical capacity position it as a promising diagnostic tool for personalised medicine and global health interventions. Remaining challenges include clinical metadata acquisition, validation of diagnostic models, and expansion of the fingerprint database for broader clinical applicability.

Acknowledgement: The authors gratefully acknowledge the financial and institutional support provided by the Slovak Agency for International Development Cooperation (SAMRS) and the Ministry of Foreign and European Affairs of the Slovak Republic. We also extend our sincere thanks to PerBiotiX s.r.o. for providing anonymised stool samples and for their collaboration in sample collection and preparation. This project "Improving public health by sending doctors, community education, providing internships and deploying an AI disease analyser and water purification equipment (SAMRS/2024/KE/1/2)" lasting from 12.2024 to 04.2026 is implemented with funds from the official development assistance of the Slovak Republic.

1. Introduction

The evolution of analytical diagnostics in medicine is increasingly driven by the need for precision, and accessibility [1]. Conventional approaches such as DNA sequencing, immunoassays, and mass spectrometry provide high-resolution data, yet remain constrained by high operational costs, dependency on laboratory infrastructure, and complex workflows. These limitations hinder their routine deployment in primary care, emergency medicine, and under-resourced environments [2]. Artificial intelligence and advanced statistical methods offer transformative capabilities in this domain. Machine

learning algorithms can extract meaningful patterns from high-dimensional sensor data with minimal preprocessing, allowing for real-time assessment of physiological or pathological states [3,4]. The QUANTUM platform exemplifies this shift in diagnostic strategy. Developed at Comenius University in collaboration with PerBiotiX and international partners, it integrates compact sensor arrays with AI models to interpret multisignal inputs from biological samples such as stool, urine, and water. The resulting signal fingerprints are analyzed using principal component analysis, clustering techniques, and probabilistic modelling to infer health conditions or disease phenotypes. This study presents the technical framework, analytical performance, and practical applications of the QUANTUM system. Particular focus is placed on the identification of gut phenotypes, the mapping of disease-related signal subclusters, and the remaining challenges associated with validation and clinical translation. The results demonstrate the feasibility of reagent-free, portable diagnostic tools that can operate outside of specialized laboratories while maintaining clinically relevant precision.

2. Materials and Methods

Stool samples were collected by a partner healthcare company in full compliance with the General Data Protection Regulation and applicable ethical standards. All specimens were stored in sterile, single-use 3D-printed inserts according to a standardized sampling protocol. Sample homogenization was performed directly within the inserts using an integrated, sterile, ultrasound-based system embedded in the QUANTUM analyzer. This method ensured uniform physical dispersion of material, minimized sample handling, and effectively eliminated the risk of cross-contamination. All biological materials were anonymized and maintained under controlled temperature conditions until analysis. The QUANTUM diagnostic platform comprises a compact analytical unit incorporating 26 distinct sensors. These include broad-spectrum optical detectors, electrochemical probes, thermal sensors, and additional non-electrical modalities, all capable of capturing physicochemical properties across multiple temporal and frequency domains. Sensor outputs are synchronized through an embedded microcontroller, which performs real-time acquisition and preliminary signal filtering. Processed data are locally stored and subsequently transferred to an AI-driven backend system for advanced analysis and classification. The entire platform operates within fully portable, reagent-free housing optimized for deployment in both clinical and field settings.

3. Results

Obtained results consist of complex, high-dimensional fingerprints that reflect the overall biochemical and physical composition of the sample. Each fingerprint undergoes processing through a multilayered analytical pipeline composed of principal component analysis, k-means clustering, neural networks, and Bayesian inference algorithms. This approach enables the classification of each sample based on pattern similarity with an expanding reference database of annotated fingerprints. The system is engineered to function without chemical reagents or laboratory infrastructure, offering a fully portable, reagent-free solution optimized for speed, simplicity, and field deployment. Cluster optimization analysis employed both the Elbow method and Silhouette score evaluation (Fig. 1). The Elbow plot revealed a sharp decline in within-cluster variance up to seven clusters, indicating $k = 7$ as the optimal solution (Fig. 1A). Although the Silhouette score reached a global maximum at $k = 2$, this solution was biologically oversimplified. A local maximum at $k = 7$ provided a more meaningful balance between intra-cluster similarity and inter-cluster separation, thereby justifying the selection of seven core gut phenotypes (Fig. 1B). Using this model, seven distinct gut phenotypes were identified through signal-based clustering of stool samples. These phenotypes were associated with characteristic microbial and metabolic signatures. Cluster 1 corresponded to protein fermentation and elevated ammonia levels. Cluster 2 was characterized by bile acid dominance and increased lipid metabolism. Cluster 3 reflected a fiber-fermenting microbiota typical of plant-based dietary patterns. Cluster 4 exhibited low microbial density commonly observed following antibiotic use or during acute diarrhoeal episodes. Cluster 5 was dominated by oxidative stress markers and is potentially linked to malignant transformation. Cluster 6 represented a balanced, normobiotic gut profile, while Cluster 7 was distinguished by pigment accumulation associated with liver–gut axis disruption (Fig. 1). In addition to phenotype-level classification, the system identified more than 20 diagnostic subclusters nested within the seven main

groups. These subclusters captured subtle yet reproducible distinctions in metabolic and microbial states and exhibited statistical correlations with clinical conditions including metabolic syndrome, hepatic impairment, inflammatory bowel disorders, and antibiotic-induced dysbiosis. Classification accuracy across subclusters ranged from 76 to 95 percent, with consistently low false positive rates between 10 and 17 percent, demonstrating strong reliability and generalizability of the model despite the absence of molecular profiling.

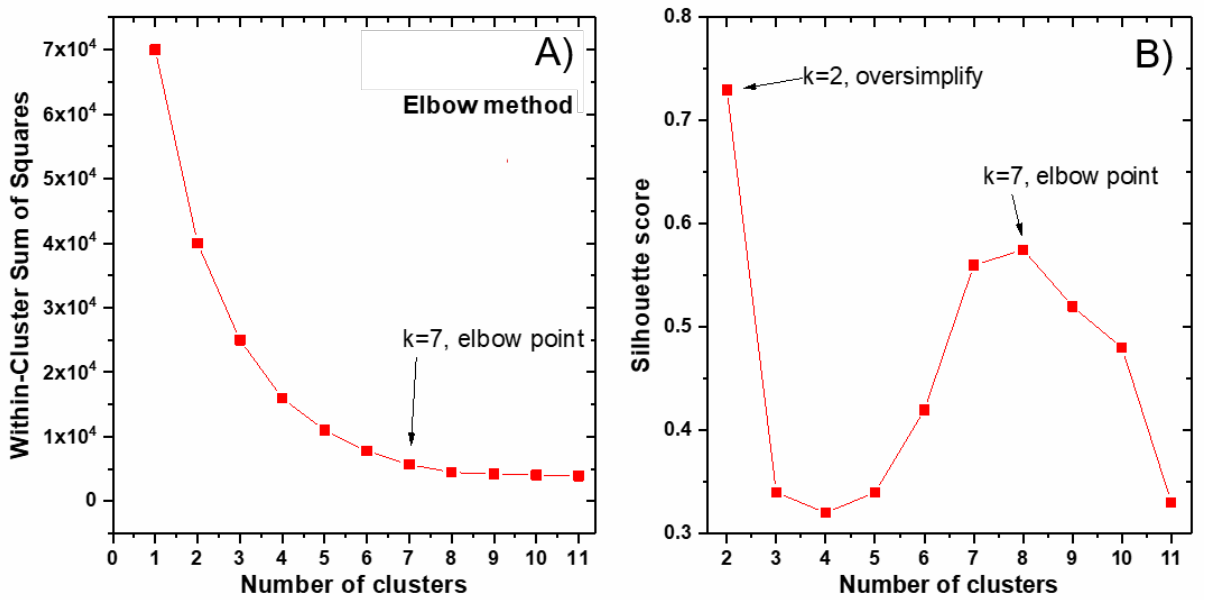

Figure 1. The **(A)** Elbow method shows a sharp reduction in within-cluster sum of squares up to k = 7, indicating this as the optimal number of clusters; **(B)** Silhouette score peaks at k = 2, but this solution is biologically too simplistic. A local maximum at k = 7 offers the best trade-off between cluster cohesion and separation, supporting the choice of seven distinct gut phenotypes.

4. Discussion

The results presented here confirm that the QUANTUM diagnostic platform has potential to identifying different gut phenotypes and disease-associated signal patterns using non-invasive, reagent-free multisensor fingerprinting. The use of unsupervised clustering techniques, supported by Elbow and Silhouette analysis, provided a statistically and biologically robust model for differentiating gut environments based on global signal features alone. The identification of seven major phenotypes reflects not only the technical resolution of the sensor system but also the underlying physiological diversity of the human gut microbiome. These phenotypes corresponded to well-described biological states, including fermentative, dysbiotic, oxidative, normobiotic, and liver-associated profiles. The clear reproducibility of these patterns reinforces the validity of fingerprint-based diagnostics as a powerful alternative to conventional assays, such as sequencing or immunochemical detection. Furthermore, the subcluster classification model adds diagnostic granularity, allowing the detection of early-stage deviations in microbial or metabolic function that may precede clinical manifestation. The achieved diagnostic performance metrics, most notably the classification accuracy of up to 95 percent and low false positive rates, highlight the platform's potential for integration into early screening and personalized medicine strategies. However, the study also underscores a fundamental limitation in the current phase of development. Although more than 6000 samples have been processed to date, many lack high-quality structured metadata, including medical diagnoses, pharmacological histories, and dietary records. Further research must therefore prioritize the systematic collection of annotated clinical datasets to validate and expand phenotype–disease correlations. In the other hand, the versatility and portability of the QUANTUM device have enabled real-world deployment in global health settings. Field testing in Kenya, focused not only on diseases, but on drinking water safety and community health monitoring, illustrates the system's robustness and adaptability in low-resource environments. These

efforts are supported by broader initiatives that combine community education, medical training, and AI-based diagnostic infrastructure. International collaborations with institutions in Slovakia, Austria, Cuba, and Canada are further enriching the platform's reference database and ensuring external validation across diverse populations. Moreover, industrial partnerships, particularly with the biotech company PerBiotiX, are exploring the clinical utility of gut fingerprinting for personalized probiotic interventions.

5. Conclusions

The QUANTUM diagnostic platform is an advanced tool that combines artificial intelligence, sensor systems, and data analytics for non-invasive health monitoring. It identifies gut phenotypes and disease-related patterns based on physicochemical fingerprints, offering a cost-effective and accessible alternative to conventional diagnostics. With over 80 percent classification accuracy and a reagent-free design, it is well suited for both clinical use and field deployment, including in low-resource settings. While early applications show promise, broader clinical adoption will require more patient data, expansion of the diagnostic database, and formal regulatory approval. Future development will aim to improve model accuracy, cover more disease states, and connect the system to cloud-based health networks. Ultimately, the goal is to establish QUANTUM as a widely usable, AI-powered diagnostic solution for personalized and public health.

References

1. Giorgi, C.; Danese, A.; Missiroli, S.; Patergnani, S.; Pinton, P. Calcium Dynamics as a Machine for Decoding Signals. *Trends in Cell Biology* **2018**, *28*, 258–273, doi:10.1016/j.tcb.2018.01.002.
1. Al-Antari, MA. Artificial Intelligence for Medical Diagnostics-Existing and Future AI Technology! *Diagnostics (Basel)* **2023**, 13(4), 688, doi:10.3390/diagnostics13040688.
2. Cordero D. The downsides of artificial intelligence in healthcare. *Korean J Pain* **2024** 37(1), 87-88. doi: 10.3344/kjp.23312.
3. Xu, C.; Jackson, S.A. Machine learning and complex biological data. *Genome Biol* **2019**, 20, 76 https://doi.org/10.1186/s13059-019-1689-0
4. R. Ma, X.; Wei, Y.; Yang, R.; Wan and H. Zhao. Adaptive Machine Learning Model for Complex Data Processing, *3rd International Conference on Data Analytics, Computing and Artificial Intelligence (ICDACAI)* **2024**, 514-519, doi: 10.1109/ICDACAI65086.2024.00099

Comparative Analysis of Artificial Intelligence Model Architectures: Strengths, Limitations, and Application Domains.

Saul Dueñas Casas [1,2], Andrej Tóth [1], Jerguš Vengríni [1]

[1] *Comenius University, Faculty of Natural Sciences, Department of Physical and Theoretical Chemistry, Ilkovičova 3220/6, 84215 Bratislava, Slovakia*
[2] *University of Matanzas "Camilo Cienfuegos", Department of Chemistry, Carretera a Varadero, Km 3.5, 44740 Matanzas, Cuba*

Artificial Intelligence (AI) has become an essential tool in the interpretation of complex, multidimensional data across scientific disciplines. This study presents a comparative evaluation of major AI model categories, including supervised learning, unsupervised learning, reinforcement learning, generative models, graph neural networks, self-supervised learning, and foundation models, with emphasis on their application in data-intensive domains such as physical chemistry. Models were assessed using analytical criteria such as data requirements, interpretability, computational cost, generalisation ability, automation potential, and scope of applicability. Visual analyses were developed to illustrate both quantitative differences and conceptual distinctions, particularly the probabilistic or deterministic behaviour of models and their capacity for local or holistic data integration. The discussion focuses on the relevance of AI for parameter estimation from high-dimensional chemical datasets, such as spectroscopic profiles, thermodynamic measurements, and molecular simulations. Additionally, user-oriented platforms like KNIME and advanced language models such as DeepSeek are highlighted for their contribution to workflow accessibility and computational reasoning. The results confirm that optimal model selection depends on task complexity, data characteristics, and domain-specific requirements. Ethical considerations are recognised as increasingly critical, particularly in relation to the use of probabilistic and generative systems in scientific and technical environments.

1. Introduction

Artificial Intelligence (AI) has become essential to modern data analysis, offering robust solutions for automation, pattern recognition, and decision-making across diverse scientific and industrial fields [1]. Its development has produced several distinct model categories, each suited to specific types of data and analytical tasks. Supervised learning models perform well in classification and regression when sufficient labelled data is available [2]. Unsupervised learning models are used to explore hidden structures within unlabeled datasets [2]. Reinforcement learning models support adaptive decision-making through continuous interaction with dynamic environments. Generative models, such as those based on transformer architectures or adversarial training, enable the synthesis of new data, including text, images, and audio, with growing relevance in scientific modelling and creative industries. In addition to these foundational approaches, advanced models have emerged to address increasingly complex data environments. Graph Neural Networks are particularly effective for data structured as graphs, such as molecular or network data. Self-supervised learning allows models to extract patterns from unlabeled datasets, improving generalization and reducing dependency on manual annotation. Foundation models, including GPT-4, PaLM, and LLaMA, demonstrate strong performance across tasks

with minimal fine-tuning. Platforms like KNIME, DeepSeek, and TensorFlow Extended further enhance the accessibility and scalability of AI tools. This work provides a structured comparison of these models and platforms, focusing on their analytical capabilities, limitations, and ethical considerations relevant to scientific research and technological deployment. In today's era of rapidly developing AI, it is increasingly necessary to consider the ethical issues associated with its use [3].

2. Materials and Methods

Seven categories of AI models were analyzed: supervised learning, unsupervised learning, reinforcement learning, generative models, graph neural networks, self-supervised learning, and foundation models. Evaluation criteria included data requirement, interpretability, computational cost, generalization, application breadth, and automation capability. Scores were assigned on a scale from 1 to 10 based on published literature, expert assessment, and relevance to chemical data analysis tasks. Figure 1 presents a comparative heatmap synthesizing these scores to highlight strengths and limitations across models. Figure 2 provides a conceptual classification along two axes: probabilistic versus deterministic behavior and local versus holistic analytical scope. This framework was based on model architecture, stochasticity in output, and capacity for contextual integration. The methods reflect typical applications in physical chemistry, including spectral analysis, thermodynamic modelling, and structure-property prediction.

3. Results

The evaluation of key AI model categories revealed clear differences in performance, adaptability, and application scope. These findings are summarized in Figures 1 and 2, which provide both quantitative and conceptual perspectives. Figure 1 presents a heatmap comparing seven AI models across six analytical criteria: data requirement, interpretability, computational cost, generalization, application breadth, and automation capability. Supervised learning models achieved high scores in interpretability and precision but showed limitations in flexibility and data dependency. Unsupervised models performed moderately across all metrics but excel in exploratory tasks with unlabeled data. Reinforcement learning demonstrated strong automation potential but was limited by high resource demands and low interpretability. Generative models achieved high scores in content creation and generalization but pose challenges in reliability and computational cost. Graph neural networks and self-supervised learning models exhibited a balanced performance profile. Foundation models outperformed others across most criteria, confirming their broad adaptability and minimal need for task-specific fine-tuning.

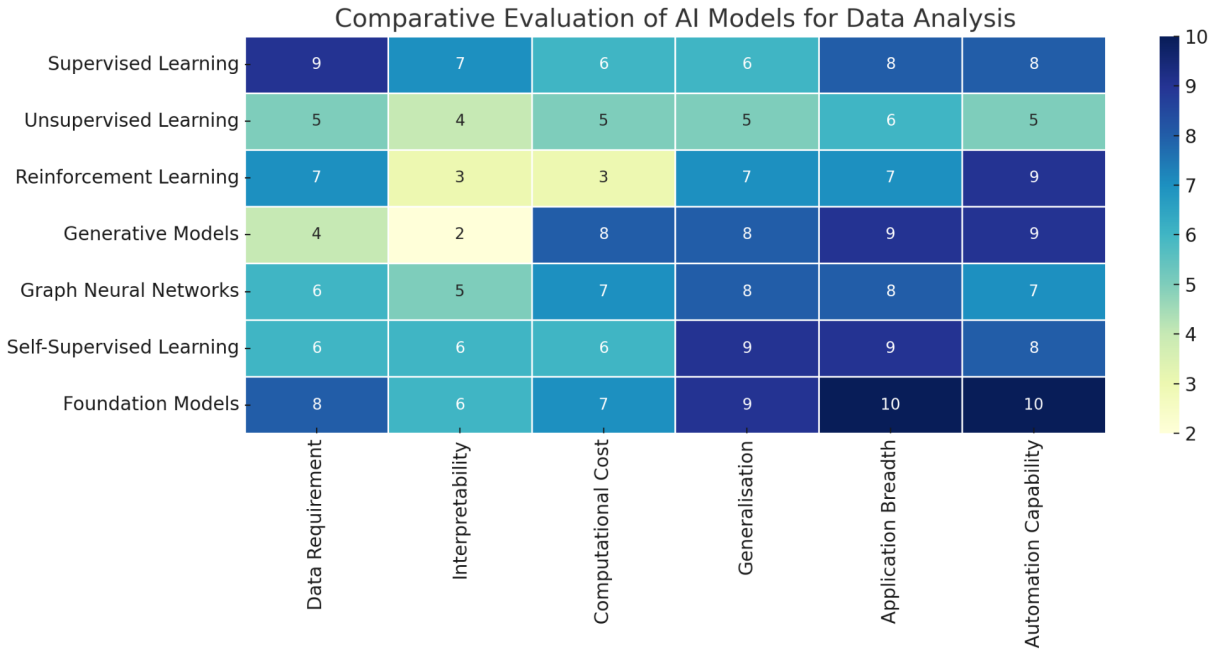

Figure 1. Comparative evaluation of seven advanced AI model categories based on six analytical criteria relevant to data analysis. The heatmap illustrates relative strengths in terms of data requirement, interpretability, computational cost, generalisation ability, application breadth, and automation capability. Higher scores indicate greater proficiency in the respective criterion. The assessment highlights the versatility of foundation and self-supervised models, while also noting the specialised advantages and limitations of traditional supervised, unsupervised, reinforcement, generative models, and graph neural networks.

Figure 2 presents a conceptual classification of the analysed AI models using a two-dimensional framework. The horizontal axis represents the spectrum between probabilistic and deterministic behaviour, while the vertical axis reflects the degree to which a model operates with a local or holistic analytical scope. This visual framework allows a deeper understanding of how different models manage uncertainty, generalisation, and context integration within analytical workflows. Traditional models, such as supervised learning, are positioned closer to the deterministic and locally focused quadrant. These models produce consistent, rule-based outputs when provided with structured input data and predefined labels. Their decision-making processes are typically transparent, making them suitable for domains that require explainable outcomes, such as clinical diagnostics, quality control, or financial auditing. However, their performance is highly dependent on the quality and volume of annotated data, and their ability to generalise to unfamiliar or complex contexts is limited. At the opposite end of the conceptual space are models such as generative networks, self-supervised systems, and large-scale foundation models. These exhibit probabilistic behaviour and possess a more holistic scope. Rather than relying on fixed rules, they learn distributions, latent relationships, and context-dependent patterns from vast datasets, allowing them to generate diverse and flexible outputs. This makes them particularly powerful in tasks involving natural language processing, image synthesis, and cross-domain reasoning. Their strength lies in contextual awareness and their ability to operate under uncertainty, but they often require significant computational resources and present challenges in terms of output interpretability and ethical validation. Models such as reinforcement learning and graph neural networks occupy intermediate positions on both axes. Reinforcement learning adapts its decision-making through iterative interaction with its environment, combining elements of probabilistic learning with goal-oriented reward structures. While not fully deterministic, its outcomes can be guided by policy optimisation, making it suitable for autonomous systems and dynamic optimisation problems. Graph neural networks, on the other hand, process structured data through iterative message-passing mechanisms, enabling relational learning across topologies such as molecular graphs or social networks. These models balance flexibility with structural constraints, making them adaptable yet interpretable in graph-structured domains. Overall, the conceptual classification shown in Figure 2 emphasises the importance of aligning model characteristics with the demands of the application domain. Probabilistic and holistic models offer advanced capabilities for complex, high-dimensional tasks where data variability is high and contextual understanding is critical. In contrast, deterministic and locally focused models remain highly effective in controlled settings with well-defined objectives and structured data. The choice of model should therefore be guided by considerations such as data availability, expected variability, interpretability requirements, and computational feasibility. This strategic alignment ensures both methodological validity and practical efficiency in AI implementation.

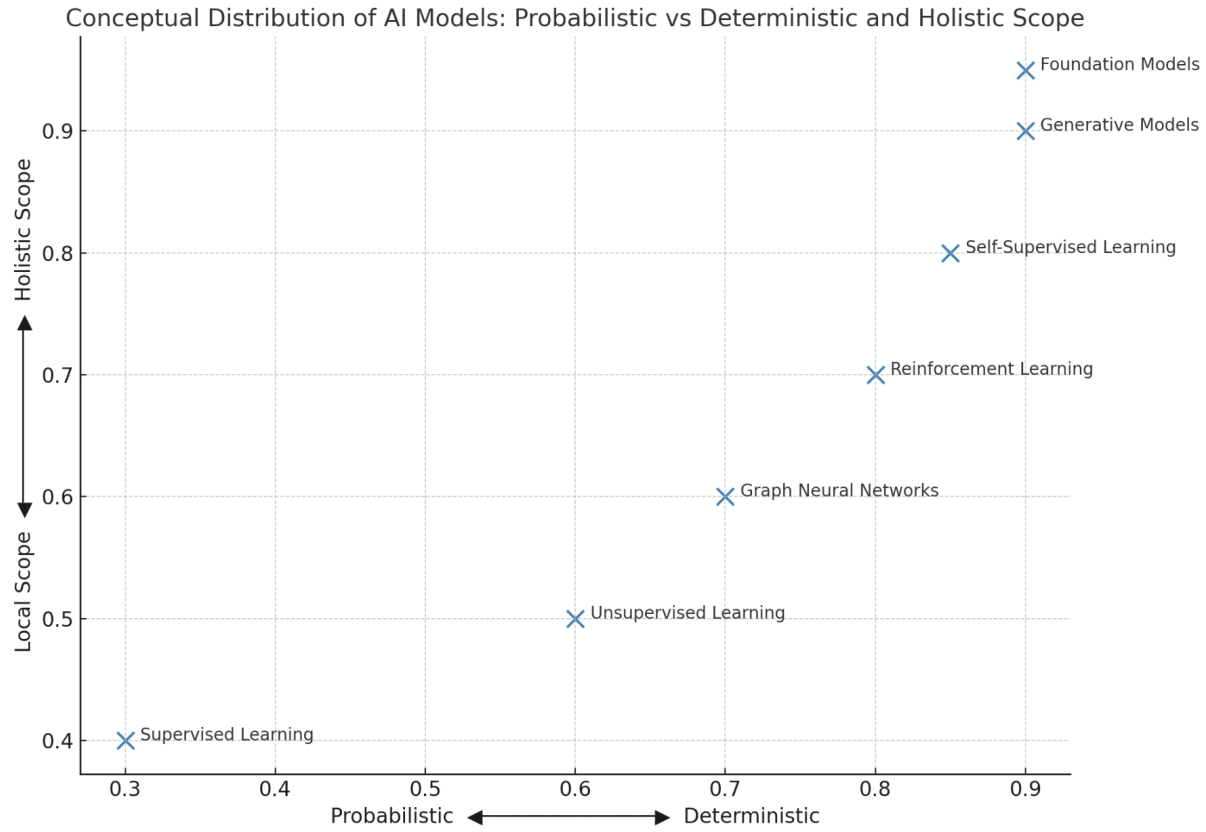

Figure 2. Conceptual mapping of AI model categories along two interpretative dimensions: probabilistic versus deterministic processing (horizontal axis) and local versus holistic analytical scope (vertical axis). Probabilistic models, such as generative and foundation models, handle uncertainty and variability, whereas deterministic models like traditional supervised learning rely on fixed, rule-based outputs. The vertical axis reflects the capacity of models to integrate context across broader data structures, with holistic models providing generalised representations and local models focusing on specific or narrowly defined features. This distribution highlights how different AI paradigms operate within the landscape of data interpretation and system design.

4. Discussion

The integration of artificial intelligence (AI) models into physical chemistry represents a transformative approach to analyzing complex, high-dimensional datasets. In fields such as spectroscopy, calorimetry, molecular dynamics, and electrochemistry, the increasing resolution and volume of experimental and computational data challenge traditional statistical tools. Modern AI architecture offers new possibilities for extracting latent variables, predicting physicochemical parameters, and modelling dynamic processes with improved precision and efficiency. Supervised learning remains a foundational technique in quantitative structure–activity relationship (QSAR) modelling, spectral deconvolution, and chemometric calibration. For example, linear and non-linear regression models trained on pre-labelled datasets can accurately predict properties such as reaction enthalpies, activation energies, or molecular dipole moments based on compositional or spectral input vectors. However, the reliability of supervised approaches is constrained by the need for extensive, high-quality training data. In many physical chemistry applications, such data are difficult to generate due to experimental limitations or system variability. Moreover, supervised models may suffer from overfitting when applied to multidimensional, collinear datasets, which are typical in spectroscopy and thermogravimetric analysis. Unsupervised learning offers a complementary approach by revealing intrinsic structures in unlabeled data. Principal component analysis (PCA), independent component analysis (ICA), and clustering algorithms can reduce dimensionality while preserving variance, allowing the identification of meaningful chemical patterns, phase transitions, or kinetic regimes. These models are particularly valuable for exploratory analysis of spectroscopic maps (e.g. FTIR, UV-Vis, or NMR datasets), where peaks and absorbance shifts reflect subtle electronic or vibrational changes. Nonetheless, the interpretability of unsupervised

models remains a challenge, as the extracted components often lack direct physical meaning without expert validation. Reinforcement learning is less common in static chemical data analysis but shows potential in dynamic optimization problems. For instance, reinforcement learning agents can be trained to simulate reaction pathways or optimize synthesis protocols in silico by maximizing target outcomes such as yield, purity, or energy efficiency. These applications require well-structured simulation environments and reliable feedback signals, which can be derived from quantum chemical calculations, thermodynamic databases, or kinetic Monte Carlo simulations. Although promising, reinforcement learning in this context is limited by computational cost and sensitivity to reward function design. Generative models such as variational autoencoders (VAEs) and generative adversarial networks (GANs) have introduced novel possibilities for simulating and extrapolating chemical behavior. These models can generate new spectra, molecular structures, or potential energy surfaces conditioned on desired properties. In physical chemistry, this can support tasks such as inverse design of materials, spectral reconstruction, and noise reduction in experimental datasets. Foundation models with transformer-based architectures further enhance these capabilities by learning long-range dependencies and correlations across multiple experimental dimensions, including time, frequency, temperature, and composition.

From the perspective of chemical parameter estimation, self-supervised and foundation models offer substantial advantages. Self-supervised learning can derive meaningful embeddings from raw spectral or structural data without requiring external labels, which is advantageous in systems where ground-truth measurements are limited. For instance, time–temperature–frequency data from dynamic mechanical analysis or variable-temperature IR spectroscopy can be encoded into latent representations that correlate with viscoelastic moduli or vibrational modes. Similarly, foundation models trained on large databases of molecular systems can infer parameters such as Gibbs free energies, solvation potentials, or rate constants by leveraging transfer learning from structurally related systems. Graph neural networks (GNNs) provide additional interpretive power by representing molecules or extended systems as graphs, where nodes correspond to atoms and edges to chemical bonds or spatial interactions. These models have demonstrated accuracy in predicting quantum-level properties, including orbital energies, partial charges, or interatomic force constants. In multidimensional chemical datasets, GNNs enable spatially resolved predictions that account for connectivity, electron delocalization, and local chemical environment, which are critical in physical chemistry contexts such as catalysis, surface interactions, or supramolecular assembly. Taken together, the application of AI models in physical chemistry demands careful consideration of data structure, target parameter complexity, and required interpretability. While traditional models offer clarity and are sufficient for linear systems with known behavior, newer architectures provide essential tools for modelling nonlinear, multivariate, and probabilistic systems. The choice of AI approach should be driven by the nature of the chemical phenomena under investigation, the dimensionality and quality of available data, and the need for predictive generalization or mechanistic understanding. Continued integration of AI with chemical domain knowledge, especially through hybrid models that combine machine learning with first-principles theory, holds the potential to revolutionize parameter estimation and accelerate discovery in physical chemistry.

5. Conclusions

This work presented a comparative assessment of key artificial intelligence models relevant to multidimensional data analysis, with emphasis on their applicability in physical chemistry. Supervised and unsupervised models remain valuable for structured datasets and exploratory tasks, respectively, while reinforcement and generative models support adaptive learning and data synthesis under variable conditions. Advanced approaches, including self-supervised learning, graph neural networks, and foundation models, offer enhanced capabilities for extracting and predicting complex chemical parameters from high-dimensional data. In physical chemistry, these models facilitate interpretation of spectroscopic, thermodynamic, and molecular data where conventional methods are limited. The choice of model should be guided by data characteristics, task complexity, and the required balance between interpretability and generalization. Integrating AI with domain-specific chemical knowledge is essential for achieving accurate, reliable, and mechanistically meaningful outcomes.

References

1. Hooman, H. R., et al. Statistics of Generative Artificial Intelligence and Nongenerative Predictive Analytics Machine Learning in Medicine. *Modern Pathology* **2024**, https://doi.org/10.1016/j.modpat.2024.100663
2. Alloghani, M., et al. A Systematic Review on Supervised and Unsupervised Machine Learning Algorithms for Data Science. In: Berry, M., Mohamed, A., Yap, B. (eds) Supervised and Unsupervised Learning for Data Science. Unsupervised and Semi-Supervised Learning. *Springer, Cham.* **2020**, https://doi.org/10.1007/978-3-030-22475-2_1
3. Ahmad, S. F., et al. Impact of artificial intelligence on human loss in decision making, laziness and safety in education. *Humanities and Social Sciences Communications* **2023**, 10, 311 https://doi.org/10.1057/s41599-023-01787-8

Integrácia prediktívnych nástrojov do manažmentu antibiotickej liečby (AMS)

RNDr. Andrej Minich, PhD.[1], Mgr. Vladimír Heger, PhD.[2], Ing. Rudolf Kubička[3]

[1]. *Medirex Group Academy n.o., Novozámocká 1, 949 05, Nitra, Slovensko*
[2]. *Heger s.r.o., Doľany, Doľany 398, 900 88, Slovensko*
[3]. *Neoxx a.s., Ružová dolina 16648/8, 821 09 Bratislava, Slovensko*

Staphylococcus patrí medzi najčastejšie patogény spojené s nozokomiálnymi infekciami, pričom jeho liečba je čoraz komplikovanejšia v dôsledku narastajúcej antimikrobiálnej rezistencie (AMR). Vysoká miera asymptomatickej kolonizácie u približne 30 % populácie zvyšuje pravdepodobnosť infekcie vlastnými kmeňmi, čo zdôrazňuje potrebu rozlišovania medzi kolonizáciou a infekciou pri interpretácii laboratórnych výsledkov. Na Slovensku však stále chýbajú systematické epidemiologické údaje, ktoré by umožnili efektívne sledovanie týchto javov v čase a priestore.

V našej štúdii sme analyzovali viac ako 100 000 záznamov z rutinných mikrobiologických vyšetrení, pričom sme využili open-source analytickú platformu **KNIME.** Zamerali sme sa najmä na multirezistentné kmene *S. aureus* a *S. epidermidis*, definované podľa štandardov ECDC. Dáta boli normalizované podľa definovaného časového obdobia a analyzované pomocou nástrojov na vizualizáciu trendov, identifikáciu klastrov rezistencie, a koreláciu výskytu s typom oddelenia.

Výsledkom tejto analýzy je vytvorenie interaktívnej aplikácie **StaphySearch**, ktorá umožňuje v reálnom čase sledovať výskyt rezistentných patogénov naprieč nemocnicami a oddeleniami a zároveň poskytuje podklady pre vyhodnocovanie ekonomického dopadu rezistencie. Aplikácia integruje viaceré dátové zdroje do používateľsky prívetivého rozhrania, čím podporuje rozhodovanie klinikov v oblasti antibiotickej stratégie (AMS) a plánovanie cielených epidemiologických intervencií.

Acknowledgement: Financované Európskou úniou z iniciatívy NextGenerationEU prostredníctvom Plánu obnovy a odolnosti Slovenskej republiky v rámci projektu č. 09I03-03-V04-00769.

Dátové inžinierstvo v biomedicíne pomocou KNIME: Skúsenosti zo Zdravotného Kompasu

Tomáš Jakuš[1]

[1] *Heger s.r.o. Doľany 398, 90088 Doľany*

S narastajúcim množstvom biomedicínskych údajov sa ukazuje ako kľúčové vybudovať spoľahlivý, automatizovateľný a auditovateľný proces ich spracovania – známy ako dátové inžinierstvo. V tejto oblasti zohráva významnú úlohu platforma KNIME, ktorá umožňuje vizuálny návrh workflowov na úrovni ETL procesov, predspracovania a prípravy dát pre štatistické alebo AI modely.

V prvej časti prezentácie ukážeme, ako KNIME podporuje štandardizáciu dátových tokov v biomedicínskom výskume. Zameriame sa na aspekty ako:

– integrácia rôznych typov dát (klinické, omické, dotazníkové),
– transformácia a čistenie údajov bez nutnosti programovania,
– reproducibilita workflowov a verzovanie výstupov,
– príprava datasetov pre klasifikáciu a predikciu pomocou AI.

KNIME sa ukazuje ako efektívny nástroj pre tímy, ktoré potrebujú flexibilitu a zároveň transparentnosť pri spracovaní údajov. V kontexte biomedicíny to predstavuje výhodu pri spolupráci medzi vývojármi, bioinformatikmi a klinickými expertmi.

V druhej časti príspevku stručne predstavíme, ako sa tieto princípy premietli do konkrétnych riešení v rámci projektu Zdravotný Kompas:

1. KNIME workflowy pre firmy a inštitúcie – predpripravené alebo personalizované dátové potrubia na analýzu výskumných alebo klinických dát,
2. Analytický tím ako služba – model spolupráce, v ktorom poskytujeme externú analytickú kapacitu na mesačnej báze, vrátane návrhu, realizácie a správy dátových workflowov.

Cieľom príspevku je poukázať na potenciál platformy KNIME v kombinácii s metodológiou dátového inžinierstva ako efektívneho riešenia pre výzvy súčasného biomedicínskeho výskumu.

Zdravotný Kompas a Vedecký Radar: Informačná inteligencia pre biomedicínsky výskum

Vladimír Heger[1]

[1] *Heger s.r.o. Doľany 398, 90088 Doľany*

Dátová záťaž vo vedeckom výskume rastie exponenciálnym tempom, čím sa stáva čoraz náročnejšie udržať prehľad o najnovších poznatkoch a relevantných publikáciách. V tejto prezentácii predstavujeme dve inovácie z dielne Zdravotný Kompas – Vedecký Radar a platformu Zdravotný Kompas – ktoré slúžia ako digitálni asistenti výskumníka v oblasti biomedicíny.

Vedecký Radar je inteligentná analytická služba postavená na platforme KNIME, ktorá monitoruje vedecké publikácie a extrahuje z nich kľúčové poznatky s dôrazom na kontext, nie len kľúčové slová. Umožňuje efektívne sledovať nové trendy, pripravovať podklady pre granty a publikácie a znižovať informačný šum vo výskumnom procese.

Zdravotný Kompas ako širšia iniciatíva prepája odborníkov z oblasti biomedicíny s dátovou a softvérovou expertízou. Podporuje vznik personalizovaných analytických nástrojov, ponúka vývoj biomedicínskych aplikácií na mieru a vytvára sieť expertov pre spoluprácu na inovatívnych výskumných projektoch.

Prezentácia poukazuje na prienik bioinformatiky, umelej inteligencie a vývoja softvéru v službách modernej vedy a ukazuje, ako môže byť dátová analytika kľúčovým nástrojom pri akcelerácii výskumného a klinického poznania.

Záverečné slovo

Milé kolegyne, milí kolegovia,
vydaním tohto zborníka rozšírených abstraktov sa symbolicky začína nielen prvý ročník konferencie **Zdravotný Kompas**, ale aj nová etapa spoločného úsilia o prepojenie **vedeckého poznania, dátovej analytiky a technologických inovácií**.
Zdravotný Kompas je novovznikajúca platforma – projekt i firma – ktorej cieľom je vytvárať priestor pre **medziodborovú spoluprácu v biomedicíne, bioinformatike a dátovej vede**. Našou ambíciou je podporovať nielen jednotlivé výskumné tímy, ale aj budovať komunitu, ktorá spoločne hľadá nové riešenia pre výzvy **modernej medicíny aj vedy ako takej**.
Tento zborník je dôkazom, že u nás existuje silný vedecký potenciál, pripravený formovať budúcnosť výskumu. Veríme, že nadchádzajúca konferencia bude miestom prvých diskusií, nových impulzov a budúcich spoluprác, ktoré nadviažu na tieto myšlienky.
Sme presvedčení, že Zdravotný Kompas má potenciál rásť – odbornou kvalitou, komunitným presahom aj praktickým dopadom. Pevne dúfame, že **o rok sa stretneme opäť – vo väčších priestoroch, v širšom odbornom zastúpení a s konkrétnymi výsledkami spoločnej práce**.
Ďakujeme za dôveru a tešíme sa na osobné stretnutia.
S úctou,
Mgr. Vladimír Heger, PhD.
Mgr. Daniel Furka, PhD., MLJ.
Mgr. Samuel Furka, PhD., MLJ.
(v mene organizačného výboru Zdravotného Kompasu)

9788097510909

Medzinárodné štandardné číslo knihy
International Standard Book Number

Heger s. r. o.

Doľany 398
900 88 Doľany

NB-OD1/2440/2025-zc 25.07.2025

Na titul: Heger, Vladimír: 1. Konferencia Zdravotného Kompasu. Zborník rozšírených abstraktov

prideľujeme ISBN 978-80-975109-0-9

s čiarovým kódom EAN 9788097510909

ISBN tak ako je uvedené v predchádzajúcom riadku má byť uverejnené na rube titulného listu, v tiráži a na obálke v samostatnom riadku a s výrazným typom písma. Za správnosť uverejneného ISBN zodpovedá vydavateľ. Ďalšie tituly, ktoré idete zadať do tlače, ohlasujte s týmito údajmi: vydavateľ, autor(i), názov, podnázov, zväzok, časť (len pri viaczväzkových dielach), poradie vydania a druh väzby.

Od začiatku verejného rozširovanie publikácie je vydavateľ povinný poslať povinné deponáty podľa Zákona č. 265/2022 Zákon o vydavateľoch publikácií a o registri v oblasti médií a audiovízie a o zmene a doplnení niektorých zákonov (zákon o publikáciách), šiesta časť, §19.

Ďakujeme.

S pozdravom

PhDr. Ľudmila Rohoňová, v.r.
riaditeľka Národnej bibliografie

* Slovenská národná knižnica
Z. Chludová

T + 421 43 2451 140
isbn@snk.sk
www.snk.sk/isbn

Slovenská národná knižnica
Národná agentúra ISMN v SR
Nám. J. Cígera Hronského 1
036 01 Martin